Check for updates

Basin Research

WILEY | IAS

RESEARCH ARTICLE

Type of Carbonate Production, Sedimentary and Tectonic Evolution of the Pliocene Mixed Carbonate Siliciclastic Unit (Macco) in the Tarquinia Basin, Central Italy

Marco Brandano[1] | Sara Ronca[1] | Alessandro Mancini[1] | Fabrizio Lirer[1] | Antonio Cascella[2] | Giovanni Luca Cardello[3]

[1]Earth Science Department, Sapienza University of Rome, Rome, Italy | [2]Istituto Nazionale di Geofisica e Vulcanologia (INGV), Pisa, Italy | [3]Department of Chemistry, Physics, Mathematics and Natural Sciences, University of Sassari, Sassari, Italy

Correspondence: Marco Brandano (marco.brandano@uniroma1.it)

Received: 29 July 2025 | **Revised:** 5 April 2026 | **Accepted:** 17 April 2026

Keywords: bioclastic calcarenite | clinoform stacking | coralline algae | facies architecture | Mediterranean Sea | mixed carbonate-siliciclastic systems | Pliocene | syn-sedimentary tectonics

ABSTRACT

The Pliocene Epoch in the Mediterranean region marks the re-establishment of open marine conditions following the Messinian Salinity Crisis and the onset of modern Mediterranean ecosystems and climate. This study investigates the 'Macco' lithostratigraphic unit exposed in the Tarquinia area (northern Latium, Central Italy), a mixed carbonate-siliciclastic succession deposited along the passive margin of the Tyrrhenian back-arc basin during the Piacenzian. Integrated facies, stratigraphic, structural and morphostructural analyses reveal syn-sedimentary growth structures associated with segmented, first-order NW-striking faults up to 3–4 km long that strike NW-SE and generate accommodation space. Second-order NE-striking faults, which are up to 0.5 km long, played a key role in controlling the lateral distribution of lithofacies and the development of localised growth structures. The 'Macco' unit records deposition on a distally steepened carbonate ramp, characterised by coralline algae and larger benthic foraminifera in the middle ramp, and significant carbonate-siliciclastic mixing in inner and outer ramp settings. Three clino-stratified wedges reflect a complex tectono-stratigraphic framework. Nonetheless, the correlation with global eustatic curves suggests that the interplay between regional tectonics and eustatic sea-level fluctuations was the primary control on sedimentary architecture during the Piacenzian.

1 | Introduction

The Pliocene in the Mediterranean area marks the return to marine conditions after the Messinian Salinity Crisis and the transition to modern Mediterranean ecosystems and climate (Rouchy et al. 2001; Garcia-Castellanos et al. 2020). During this crucial Epoch, interactions between carbonate factory activity, detrital input and tectonics resulted in sedimentary successions, whose interplay between sedimentological and tectonic processes has not been fully investigated. In particular, the interaction between aggradation or progradation of the sedimentary wedges at the outcrop scale, with the development of passive margin syn-sedimentary growth structures has not been documented in detail for the Mediterranean Pliocene successions. While depositional geometries influenced by syn-sedimentary fault activity have been extensively studied in Mesozoic and Cenozoic carbonate successions of the Southern Tethys and central Mediterranean area (e.g., Bernoulli 2001; Cosentino et al. 2010; Carminati et al. 2013; Cardello and Doglioni 2015; Manatschal et al. 2022; Tavani et al. 2023), the Pliocene successions on the passive margins of the Tyrrhenian Sea, one of the major and younger back-arc basins of the Mediterranean basin, has received less attention.

Along the northern and central coasts of the Tyrrhenian Sea bounded by the Apennines (Figure 1), the Pliocene sedimentary

© 2026 International Association of Sedimentologists and European Association of Geoscientists and Engineers and John Wiley & Sons Ltd.

Highlights

- Syn-sedimentary structures in the deposition of shallow-water sediment during late Pliocene Tarquinia peri-Tyrrhenian half-graben basins.
- Carbonate-Siliciclastic mixing due to coastal erosion and episodic fluvial inputs.
- The Macco unit comprises three stacked prograding carbonate wedges.
- Main control of stratigraphic architecture of Macco unit is the eustatic sea level.
- fluctuations.
- Biostratigraphy places the 'Macco' unit in the *Globorotalia crassaformis* Subzone (MPI4b).

succession includes a shallow-water bioclastic wedge that has been identified under various formational names such as '*Amphistegina* Limestone', 'Tarquinia Limestone' and 'Macco' (Di Bella et al. 2005; Nalin et al. 2016, 2010). The study area consists of a Pliocene sedimentary succession exposed on terraced cliffs edging the town of Tarquinia and its archeological sites in northern Latium (Figure 1). This mixed carbonate-siliciclastic succession, named 'Macco' (Fazzini et al. 1972), documents the evolution of a peri-Tyrrhenian basin on the Italian peninsula in a time period comprised between 3.15 to 2.33 Ma including the late Piacenzian (latest Pliocene; cf. Di Bella et al. 2005; Bulian, Marra, et al. 2024; Buttinelli et al. 2014, 2024).

Mixed carbonate-siliciclastic successions such as 'Macco' are of particular interest because they are the product of sedimentary environments that were typically sensitive to the climatic and oceanographic conditions of the sedimentary basin (Schlager 2005; Pomar 2020; Reijmer 2021), marking specific environmental conditions in the central Mediterranean. This unit is also laterally interfingered by siliciclastic deposits of the 'Pian della Regina' Lithostratigraphic unit, highlighting a complex paleogeographic distribution with compositional changes along the ancient coastline. This was generated by sedimentary processes admixing siliciclastic and carbonate inputs producing continental and shallow marine clastic successions (Mount 1984; Tortora 1996; Pascucci et al. 2006; Brogi et al. 2011). The complexity of the paleophysiography resulting from the extensional tectonic setting complicates the development of a unified depositional model for the bioclastic unit (e.g., Nalin et al. 2016), where coralline algae represent one of the primary sediment-producing biota during a time interval traditionally associated with a decline in their productivity (Aguirre and Braga 2024).

The aims of this study are: (i) to develop a depositional model for the 'Macco' unit of Tarquinia in northern Latium; (ii) to identify the controlling factors influencing the cyclicity and the resulting tectono-stratigraphic architecture; (iii) to understand the factors governing the change in the shallow-water carbonate production within the Pliocene context of the broader central Mediterranean region.

2 | Geological Setting

2.1 | Tectonics

The Tyrrhenian Sea hosts several marine basins formed by back-arc extensional processes that have shaped its physiography (Figure 1a). These processes were triggered by the westward subduction of the Adriatic microplate (Malinverno and Ryan 1986; Patacca and Scandone 1989; Doglioni 1991; Savelli 2002; Chiarabba et al. 2023). The back-arc extension disrupted the Apennine orogen on the upper plate (Faccenna et al. 1996; Jolivet et al. 1998; Sartori et al. 2004; Carminati and Doglioni 2005; Acocella and Funiciello 2006; Tavani et al. 2021; Cardello et al. 2022).

In northern Latium, crustal extension already initiated during the late Burdigalian, although it reached the most significant activity during the Serravallian to early Messinian (Buttinelli et al. 2014). During the late Messinian–Early Pliocene, the Latium offshore underwent a transition to extensive regional subsidence, characterised by the progressive basin filling and successively flattening of previously articulated geometries resulting from the extensional tectonic (Bartole 1995; Pascucci and Martini 2002; Pascucci 2005; Buttinelli et al. 2014). The locus of active extension continued to migrate towards the east to the present onshore area, where a voluminous volcanic activity mainly developed during the Plio-Pleistocene (Branca et al. 2023). Extension affecting the Tyrrhenian margin reached the internal Apennines during the Early Pliocene–Early Pleistocene (Bulian, Marra, et al. 2024) and finally exhumed part of the back-arc basinal successions during the Pleistocene. A synthetic sketched cross-section of the geological setting is provided by Buttinelli et al. (2014), who considered several public seismic lines to underpin the semi graben structure affecting the continental shelf (Figure 1b,c). In this context, the structural high hosts thin and discontinuous Pliocene–Pleistocene successions, while depocenters contain a thicker and continuous wedge.

In this frame, the Plio-Pleistocene NW-SE trending basin of Tarquinia (Fazzini et al. 1972; Barberi et al. 1994; Carboni et al. 1994; Chiocchini and Potetti 1998; Chiocchini and Castaldi 2009) is about 27 km wide and extends nearly 40 km along the Tyrrhenian margin of Latium (Figures 1, 2). The substrate of the basin consists of Meso-Cenozoic carbonate and siliciclastic units belonging to the Tuscan and Subligurian domains that have been involved in the Apennine fold-and-thrust formation. The basins are structured into several half-graben that are predominantly NW–SE oriented, with some NE–SW oriented (Figure 1). These basins were filled with syn- and post-rift clastic sediments of the Plio-Pleistocene interval (Funiciello et al. 1976; Mariani and Prato 1988), together with volcanic pro ducts from the Tuscan and Roman Magmatic Provinces (Locardi 1986; Bulian, Genesini, et al. 2024; Bulian, Marra, et al. 2024). An extensional growth fault system at the base of the 'Macco' unit has been described by Balsamo et al. (2008), who highlighted the presence of three-dimensional geometries of growth strata indicating fault propagation during extension with the formation of isolated syn-sedimentary subsidiary faults (displacement > 1 m) and dilation bands in soft-sediment conditions.

13652117, 2026, 3, Downloaded from https://onlinelibrary.wiley.com/doi/10.1111/bre.70109 by University Di Roma La Sapienza, Wiley Online Library on [05/05/2026]. See the Terms and Conditions (https://onlinelibrary.wiley.com/terms-and-conditions) on Wiley Online Library for rules of use; OA articles are governed by the applicable Creative Commons License

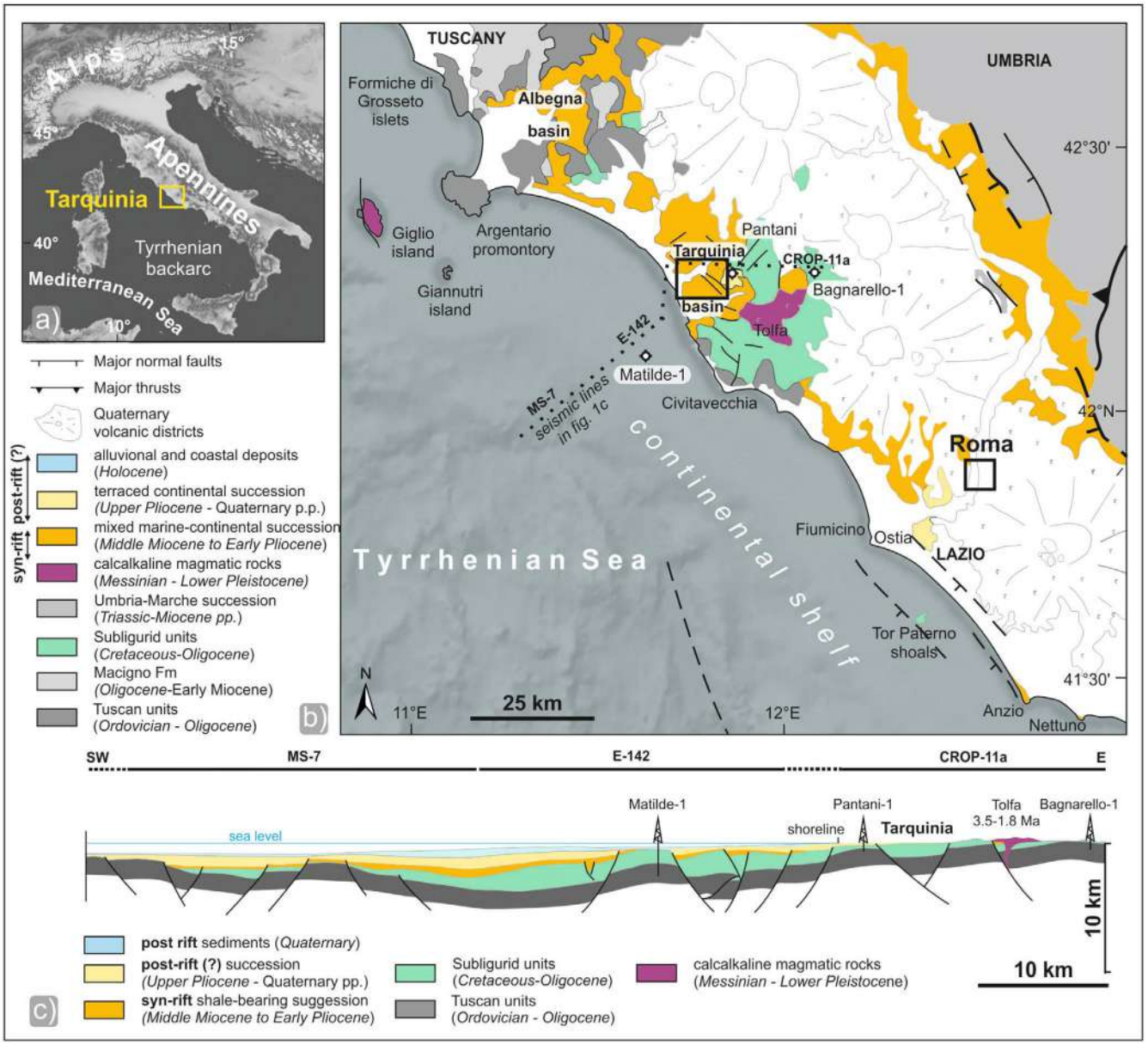


FIGURE 1 | Geological context. (a) The inset shows the geodynamic of the study area along the passive margin of the Tyrrhenian back arc. (b) Sketch tectonic map of central Italy in northern Lazio (Central Italy). (c) Conceptual structural section of the shallow crustal setting, showing the location of syn- to post-rift sediments, modified from Buttinelli et al. (2014).

2.2 | Stratigraphy

The Tarquinia Basin succession begins with about 50 m of Messinian continental conglomerates (Chiocchini and Castaldi 2009). These are covered by three depositional cycles of marine deposits. A widespread marine transgression marks the onset of the first depositional cycle. This transgression led to the deposition of clay deposits within the planktonic foraminiferal biozone *Sphaeroidinellopsis* s.l. (MPl1) to *Globorotalia puncticulata* (MPl4a) subzones (Zanclean, 5.33–3.57 Ma) of Lirer et al. (2019). These deposits can be up to 2500 m thick (Bulian, Marra, et al. 2024). According to Chiocchini and Castaldi (2009) the first cycle is bounded by stratigraphic unconformities and represented by the Zanclean platform pelites of the S. Savino System.

The second cycle is attributed to the Piacenzian *pro parte*-early Gelasian of the Tarquinia System, which includes two heteropic subsynthems: the Poggio Gallinaro sand subsynthem and the 'Macco' subsynthem. These subsynthems rest unconformably on the sediments of the first cycle or directly on the substrate (*Pietraforte*, Figure 2). The boundary is marked by a sharp facies change, and a hiatus estimated between 0.3 and 0.4 Myr (Barberi et al. 1994). The 'Macco' unit is characterised by a transgressive–regressive (T-R) cycle, chronologically corresponding to the *Globorotalia crassaformis* subzone (MPl4b)-*Globorotalia bononiensis/Globorotalia inflata* subzone (MPl5b) interval (3.59–2.29 Ma, Lirer et al. 2019) *Globorotalia aemiliana* zone p.p. (Iaccarino 1985) in Barberi et al. (1994). This cycle developed after a significant sedimentary hiatus, which is clearly visible in the Tarquinia and Albegna basins.

13652117, 2026, 3, Downloaded from https://onlinelibrary.wiley.com/doi/10.1111/bre.70109 by University Di Roma La Sapienza, Wiley Online Library on [05/05/2026]. See the Terms and Conditions (https://onlinelibrary.wiley.com/terms-and-conditions) on Wiley Online Library for rules of use; OA articles are governed by the applicable Creative Commons License

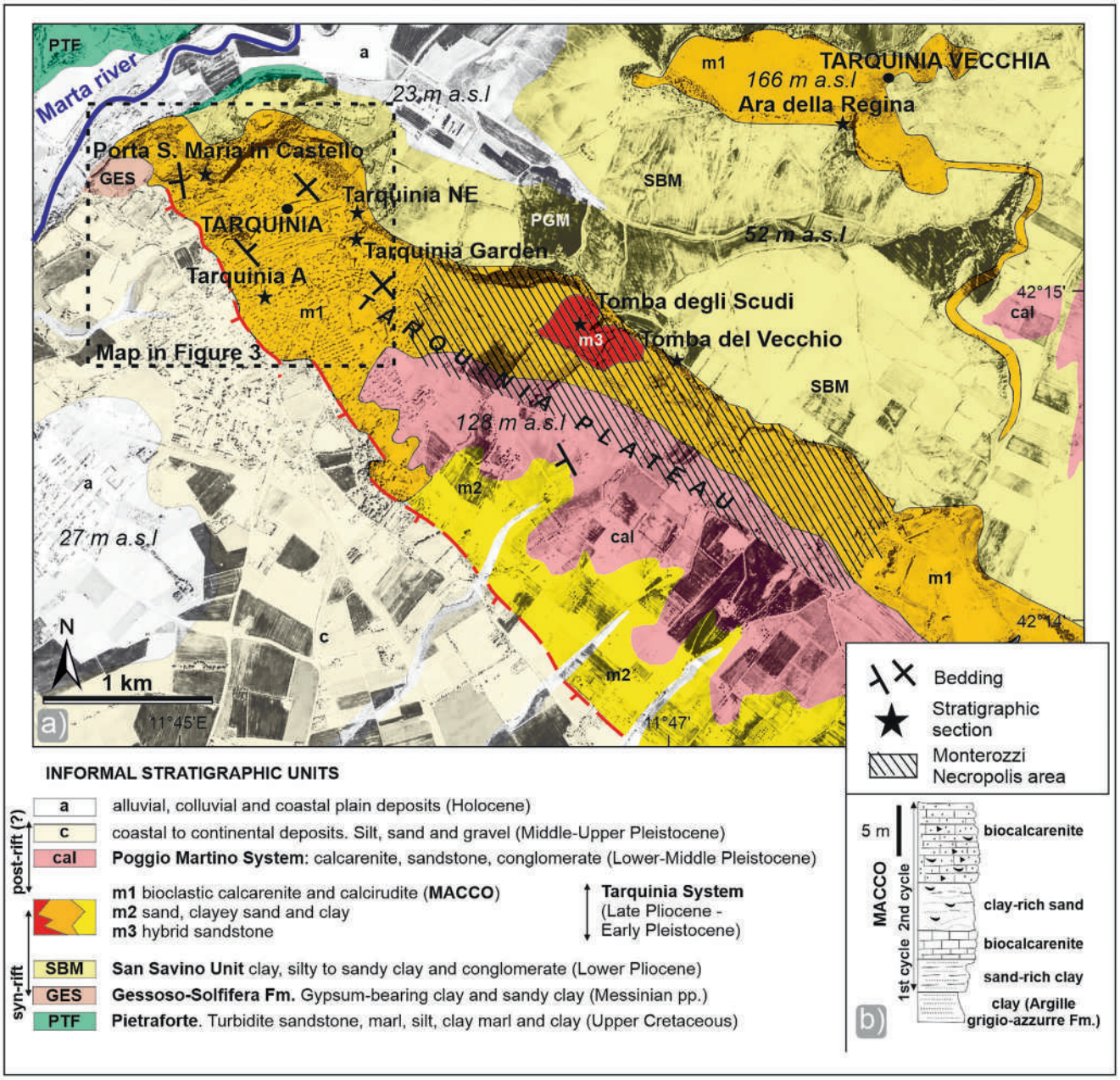


FIGURE 2 | (a) Sketch geological map of the town of Tarquinia and surrounding areas showing the Macco outcrops (simplified from Servizio Geologico d'Italia, 2020) and location of the stratigraphic sections presented in this study; (b) simplified stratigraphic section (Balsamo et al. 2008).

This hiatus (Bulian, Marra, et al. 2024) corresponds to part of the *G. puncticulata* subzone (MPl4a) of Lirer et al. (2019) and locally affects the *G. puncticulata*/*Globorotalia margaritae* biozone (MPl3) of Lirer et al. (2019). Towards the basin depocenter, the 'Macco' unit interfingers with the bioclastic sands and clays of the Pian della Regina lithostratigraphic unit, reflecting sedimentation in a circalittoral environment (Conti et al. 1983; Mazzini et al. 2000). The T-R cycle has been analysed by several authors, particularly in the Monte Riccio area (Fazzini et al. 1972; Colalongo et al. 1973; Conti et al. 1983; Mazzini et al. 2000). These studies described the 'Macco' as a 30 m thick succession of calcarenites and biodetrital sands known in the regional geological literature as 'Tarquinia calcarenite' or 'Tarquinia limestone' (Fazzini et al. 1972). Subsequently, Conti et al. (1983) identified a level rich in benthic foraminifera *Amphistegina* within the 'Macco' recognised throughout all central Italy.

In the Tarquinia area, the 'Macco' subsynthem is made up of a lithostratigraphic unit that constitutes the rocky substrate of the Etruscan necropolis of Monterozzi, a UNESCO site since 2004. This necropolis consists of more than 6000 burials of different typologies (room tombs, pit tombs and hole tombs), covering a time period from the 7th to the 2nd century BC (Cataldi 1993). Most tombs were excavated in a lithofacies represented by red algal-rich calcarenites, which can be ascribed to the 'Macco' unit (Caneva et al. 2020).

Finally, the third cycle, described by Chiocchini and Castaldi (2009), comprises the sandy and gravelly succession of

13652117, 2026, 3, Downloaded from https://onlinelibrary.wiley.com/doi/10.1111/bre.70109 by University Di Roma La Sapienza, Wiley Online Library on [05/05/2026]. See the Terms and Conditions (https://onlinelibrary.wiley.com/terms-and-conditions) on Wiley Online Library for rules of use; OA articles are governed by the applicable Creative Commons License

the Lower Pleistocene Poggio Martino System. This cycle unconformably overlies the S. Savino and Tarquinia systems.

3 | Methods and Analysis

The outcrops exposed on the cliffs of Tarquinia provide a good opportunity to analyse lithofacies, bedding geometries and facies associations. As depicted in Figures 2 and 3, seven stratigraphic sections (Tarquinia A, Tarquinia NE, Tarquinia Garden, Ara della Regina, Porta *S. Maria* in Castello, Tomba degli Scudi and Tomba del Vecchio) were measured and sampled. Stratigraphic and sedimentological interpretations were implemented by mapping lithofacies on outcrop photographs, producing two transects (Tarquinia road wall, Tarquinia garden wall). The intensity of bioturbation was measured by the Bioturbation Index (BI) following Taylor and Goldring (1993).

Bedding attitude attributes were acquired in the field. To elucidate fault kinematics, a structural field survey was conducted, capturing measurements of folds, faults, fractures and slicken fibres at key locations. These data were processed using TectonicsFP (Ortner et al. 2002), employing lower hemisphere projections and rose diagrams for visualisation. Specifically, at each locality, eigenvectors were computed from bedding data, providing insights into the orientation of deformation axes.

A morphostructural interpretation is based on tracing the break-in-slope features that were arbitrarily recognised within the dotted square in Figure 4. This analysis enables these forms to be qualitatively attributed to near-surface fault traces that cut through the surface lineament map of Tarquinia, which was generated using high-definition satellite images, allowing for local control over digitised structures. By the use of the FracPaQ toolbox (Healy et al. 2017), a multiscale analysis of fracturing was conducted on the outcrops near the Middle age walls of Tarquinia (Figures 1, 2).

Field observations were complemented by the study of over 40 thin sections for textural characterisation and identification of skeletal components. Polarised light microscopy (PLM) observations were carried out on thin sections at the *Dipartimento di Scienze della Terra* of the Sapienza University of Rome using Olympus BX50 and Zeiss AxioPhot microscopes.

In terms of calcareous plankton biostratigraphy, five samples (PG1, DX12P, DX11P, TXGA, TX10) from two stratigraphic sections (Porta *S. Maria* in Castello and Tarquina NE) have been examined.

A qualitative analysis on planktonic foraminifera was based on surveying the size fraction of washing residue >125 μm. The samples are treated and disaggregated with hydrogen peroxide diluted to 20% H_2O and the washing residue over 63 μm is dried in a 40°C oven and after sieved at 125 μm. The taxonomic planktonic foraminiferal identifications were based on Iaccarino et al. (2007).

Concerning the calcareous nannofossils, analyses were performed on standard smear slides prepared following the method described in Bown et al. (2004), using a light polarised microscope at 1250× magnification. The abundance of index nannofossils was evaluated as number of specimens per field of view (FOVs), in at least 200 FOVs, as follows: abundant (>10 per FOV), common (5–10 per FOV), few (1–5 per FOV), and rare (<1 per FOV). In this paper, we adopted for planktonic foraminifera the Neogene-Quaternary Mediterranean biostratigraphic scheme proposed by Lirer et al. (2019) and for calcareous

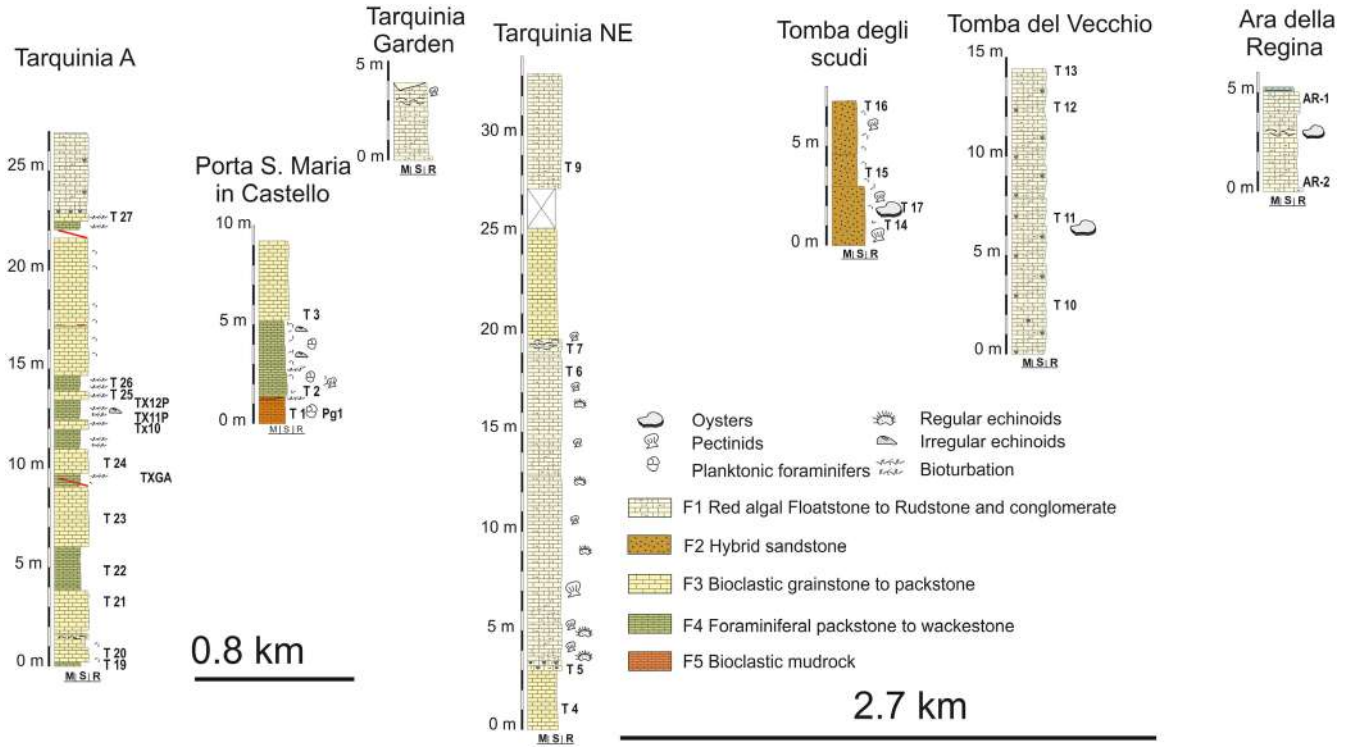


FIGURE 3 | Measured stratigraphic sections plotted against depth with sample position. Location of sections is given in Figure 2.

13652117, 2026, 3, Downloaded from https://onlinelibrary.wiley.com/doi/10.1111/bre.70109 by University Di Roma La Sapienza, Wiley Online Library on [05/05/2026]. See the Terms and Conditions (https://onlinelibrary.wiley.com/terms-and-conditions) on Wiley Online Library for rules of use; OA articles are governed by the applicable Creative Commons License

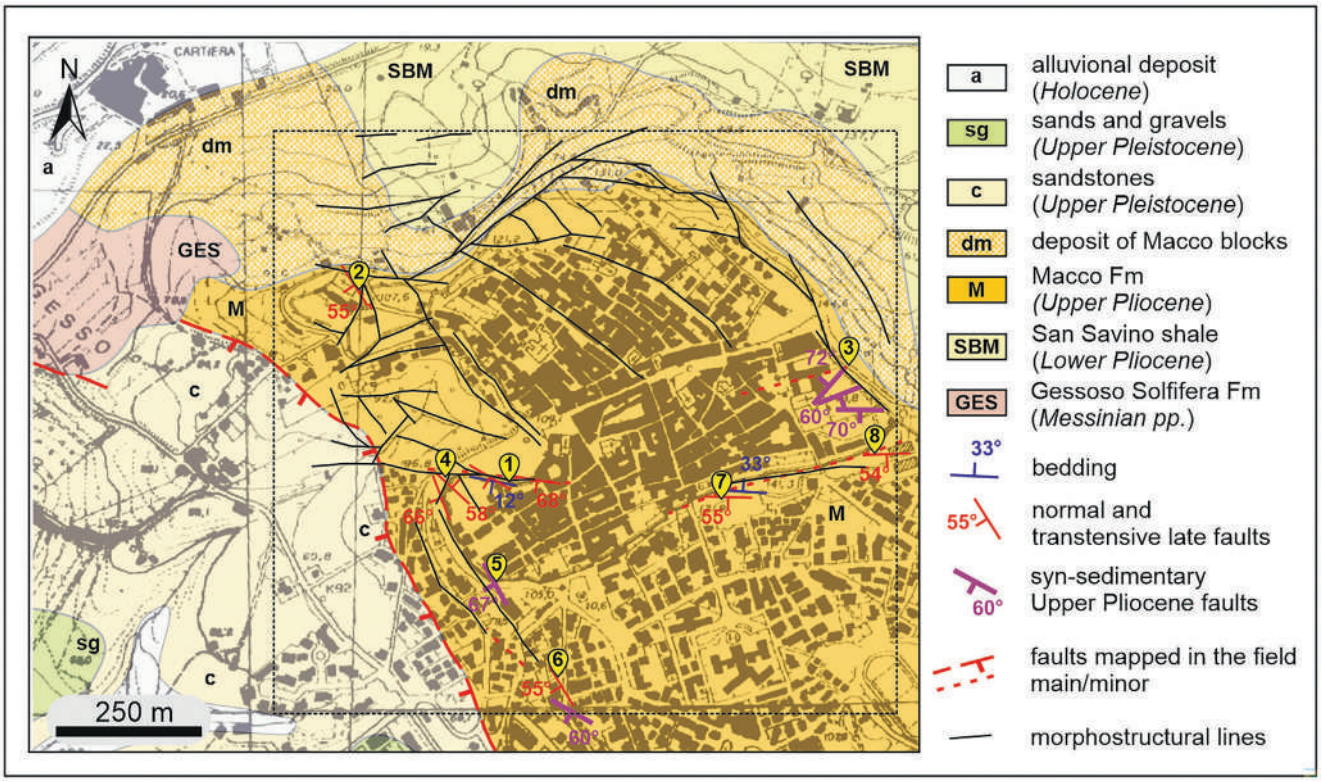


FIGURE 4 | Detailed geological map of the lithostratigraphy of Tarquinia. Fault systems are shown as red lines, while syn-sedimentary faults are shown as purple lines. Uncertain fault traces are dashed, while morphostructural lines are black. Synsedimentary evidence is marked by violet signs. Numbers are referred to structural measurement stations. The dotted square defines the area investigated though morphostructural study.

nannofossils we used the Mediterranean biostratigraphic scheme of Di Stefano et al. (2023), based on Mediterranean bio-chrono-magnetostratigraphic constrained sections.

4 | Results

4.1 | Geological Mapping

The geological map shown in Figure 4 was obtained by combining geological data from literature (see Section 2) and the new field work. It provides a detailed representation of the fault systems in the area, including the most significant syn-sedimentary faults.

4.2 | Sedimentary Facies

Seven stratigraphic sections and two transects along the road and the public garden of Tarquinia were analysed (Figure 3). Five main facies have been recognised based on variations in lithology, textural characteristics, sedimentary structures, skeletal components and microfauna assemblages.

4.2.1 | F1 Red Algal Floatstone to Rudstone and Conglomerate

This facies is dominated by coralline algal and by a skeletal debris represented by molluscs, bryozoans, echinoids and an abundant foraminiferal microfauna. The algal component is represented by free-living branches of coralline red algae, up to 1.5 cm long and 5 mm in diameter (Figure 5a,d), often displaying borings and staining of thalli and scattered rhodoliths. These latter are rare and small in size (maximum 5 cm, average 1.5–2 cm) and show subspherical shape with compact and protuberant structure. The red algal thalli are mainly constituted by melobesioids and more rarely by lithophylloids. Mollusc shells are mainly represented by bivalves (*Ostrea lamellosa*, *Chlamys opercularis, Chlamys seniensis*, *Chlamys multistriata*, *Pecten jacobaeus*, *Pecten bipartitus*, *Pecten flabelliformis*, *Spondylus* sp.), and subordinately by gastropods. The matrix consists of bioclastic packstone-grainstone and more rarely wackestone, with benthic and planktonic foraminifers, and mollusc, bryozoan (Celleporids), ostracods and red algal fragments. The foraminiferal assemblages are characterised by miliolids, rotaliids (*Lobatula lobatula, Neoconorbina, Ammonia, Elphidium*) and textularids. Disarticulated bivalve shell lags are common and consist primarily of fragmented pectinid shells. Bioturbation is pervasive, and *Thalassinoides* traces are evident along some horizons. The intensity of bioturbation can be estimated as moderate (BI 3). On the basis of stratification pattern and syn-sedimentary deformation, three sub facies can be recognised. In the F1a, plane-parallel bedding is well distinguishable. This subfacies is organised in massive tabular beds, up to 3 m thick. The subfacies F1b is characterised by meter thick composite beds showing internally foreset beds (Figure 5b), ranging from 5 to 15 cm thick, and show alternating layers of rudstone and grainstone. Intense bioturbation can baffle the stratification, giving the foresets a nodular appearance. At the Tarquinia Garden wall outcrop, the

13652117, 2026, 3, Downloaded from https://onlinelibrary.wiley.com/doi/10.1111/bre.70109 by University Di Roma La Sapienza, Wiley Online Library on [05/05/2026]. See the Terms and Conditions (https://onlinelibrary.wiley.com/terms-and-conditions) on Wiley Online Library for rules of use; OA articles are governed by the applicable Creative Commons License

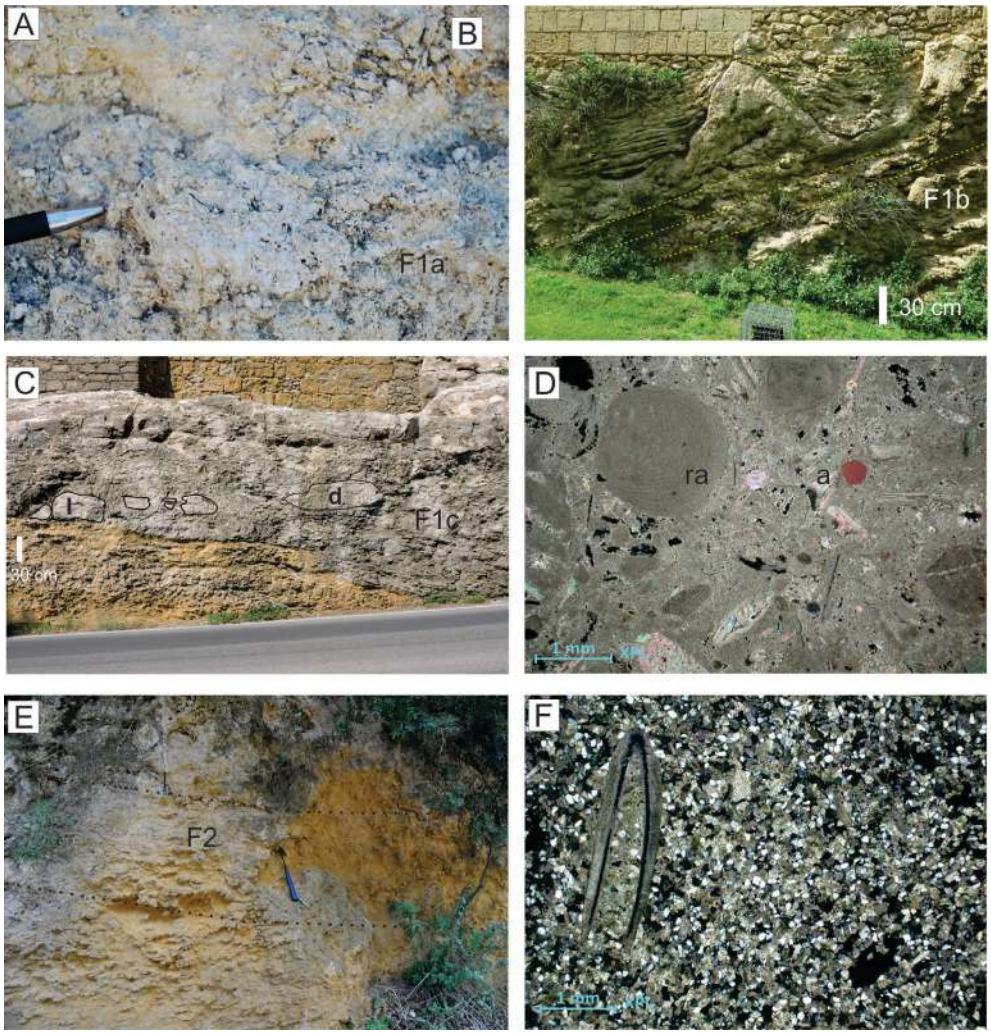


FIGURE 5 | Facies characters of Macco unit. (A–D) Facies F1 Red algal floatstone to rudstone and conglomerate; (A) F1a lacks sedimentary structures and is dominated by free-living red algal branches; (B) F1b characterised by massive to plane-parallel stratified foresets. In some areas, the tops of these beds are truncated by distinct lenticular concave structures that are unconformably filled by overlying bioclastic sediment; (C) F1c appears deformed, having been dislocated from its original depositional position, this subfacies is often associate with conglomerates whose composition is generally similar to the Red algal Floatstone to Rudstone facies (F1a and F1b) for both matrix llithoclasts (l). Deformed clasts (d) indicate that they were only semi lithified before erosion and transport; (D) thin sections of F1 showing red algae (ra), skeletal components include benthic foraminifers such as *Amphistegina* (a), rotaliids and various skeletal debris, (E, F) Facies F2 Hybrid arenite. (E) homogeneous beds due to intense bioturbation (BI 4–5); (F) thin section of F2.

tops of these beds are truncated by distinct lenticular concave structures, with depths ranging from 0.9 to 1.3 m and in length from 1 to 3 m. These concavities are unconformably filled by overlying bioclastic sediments, with parallel bedding up to 5 cm thick, draping the cavities upward (Figure 5b). There is no significant textural or compositional difference inside or outside the concave structures. Locally, the subfacies 1a and 1b appear deformed having been dislocated from their original depositional position and constituting the subfacies F1c (Figure 5c). They are identical to their parent lithofacies from a lithological point of view, but internally the original bedding is slightly to severely deformed. These deposits are typically preserved as lenticular bodies up to 5 m thick and 100 m wide. Slide dislocation surfaces and intraformational erosion surfaces are common. It is characterised by conglomerates whose composition is generally similar to the Red algal Floatstone to Rudstone facies (F1a and F1b) for both matrix and clasts. Clasts are rounded to subangular, and range in size from 1 cm to 50 cm. Some of them are tabular in shape and represent reworked and contorted fragments of beds. Deformed clasts indicate that they were only semi lithified before erosion and transport. The matrix is structureless or shows folded bedding. The conglomerates present a chaotic internal fabric and show no evidence of grading.

4.2.1.1 | **Interpretation.** Free-living red algal branches are a classical component of the Mäerl facies that develops in low-energy shallow water conditions, generally basin ward of a seagrass facies belt (Steneck 1986; Basso et al. 2017; Brandano et al. 2019) or interfingered with it. In F1a, the lack of abrasion on algal branches point to their limited transport. However, the presence of erosional scours, crossbedding and beds with grainstone matrix suggests that the seafloor was occasionally affected by moderate- to high energy events. Fluctuating hydrodynamic conditions could explain the alternation of floatstone

13652117, 2026, 3, Downloaded from https://onlinelibrary.wiley.com/doi/10.1111/bre.70109 by University Di Roma La Sapienza, Wiley Online Library on [05/05/2026]. See the Terms and Conditions (https://onlinelibrary.wiley.com/terms-and-conditions) on Wiley Online Library for rules of use; OA articles are governed by the applicable Creative Commons License

and rudstone beds, where floatstone and rudstone textures may represent autochthonous and parautochthonous accumulations, respectively (Braga et al. 2006; Nalin et al. 2010). This interpretation is consistent with the recurrent occurrence of shell lags in the algal rudstone beds, where preservation of distal tempestites consisting of slightly displaced oligotypic pectinid communities are more expected (Puga-Bernabéu et al. 2007; Nalin et al. 2010). Low bioturbation intensity (BI 1) suggests dominance of physical sedimentary structures over biogenic ones, reflecting high sediment transport rates.

Based on its compositional and textural characteristics, this facies can be attributed to an oligophotic carbonate factory. According to Pomar's classification (Pomar 2001, 2020), it would be positioned within the middle ramp.

In general, in the Cenozoic ramps, the Mäerl facies deposited in the middle ramp (c.f. Pomar et al. 2017; Brandano et al. 2019). The concave structures observed at the Tarquinia Garden Wall outcrop are interpreted as evidence of benthic foraging behaviour by marine vertebrates, particularly cetaceans. Recent studies of modern seafloors, in both shallow and deep waters worldwide, have also identified similar pits (Schneider von Deimling et al. 2023). Finally, the deformed portions observed in this facies appear to be the result sediment gravity flow processes and slumping. This dislocation probably relates to the extensional syn-sedimentary tectonic features that produced grabens (see Section 4.5).

4.2.2 | F2 Hybrid Arenite

It consists of well to moderately sorted hybrid arenite, crudely bedded with local plane-parallel to low angle crossed planar stratification. Beds, up to 2 m thick, show a homogenous aspect (Figure 5e), due to intense bioturbation (BI 4–5). The siliciclastic component consists of subangular to subrounded, medium to coarse-grained sand composed of monocrystalline grains of quartz, sedimentary lithoclasts (arenites, siltites) and subordinate micas and feldspars along with rare glauconite grains and opaques such as iron oxides and glauconite representing the main authigenic minerals (Figure 5f). The carbonate component consists of a skeletal debris mainly composed of bivalves, echinoids, serpulids (*Ditrupa arietina*) and gastropod fragments. Benthic foraminifers include rotaliids (*Elphidium*, *Lobatula*, *Ammonia beccari*), discorbids (*Neconorbina*) and rare *Amphistegina* specimens. Disarticulated ostreid shells, sparse red algal branches, are locally observed (Figure 5f). Intergranular spaces are filled with microsparite cement and more rarely by fine-grained (mostly micritic) matrix. A distinctive feature is the high ratios of authigenic mineralisation in skeletal cavities and on outer surface.

4.2.2.1 | Interpretation. The mixture of terrigenous particles with parautochthonous skeletal production supports a moderate-energy environment with a significant land-derived input, with periodic disturbance of the bottom sediment, close to emerged landmass or fluvial input. This is confirmed by a rather poor epiphytic benthic foraminiferal assemblages dominated by *Elphidium, Lobatula* and *Ammonia beccari*. This last foraminifer lived in conditions of fluctuating salinity such as those of river estuaries. Similar to today, frequently *Ammonia* occurs associated with *Elphidium* and *Lobatula*, which characterise the nearshore or inner ramp, estuarine or paralic facies vegetated by seagrass (Jorissen 1988; Haynes 1992; Murray 2006; Dupuy et al. 2010; Consorti et al. 2020). The abundance of *Ditrupa* is also consistent with this environment. This genus is a short-lived, free-living, tusk-shaped tube, suspension-feeding serpulid, indicative of high sedimentation/turbidity and unstable mixed substrates, sensitive to increasing concentrations of fine sediments, and rather tolerant to the presence of coarse sediments (Grémare et al. 1998; Cosentino and Giacobbe 2006). Along the shelf, it can easily constitute oligotypic associations, which are recorded in many modern and fossil marine benthic stressed ecosystems (e.g., Bernasconi and Robba 1993; Labrune et al. 2006; Morton and Salvador 2009).

4.2.3 | F3 Bioclastic Packstone to Grainstone

This facies is characterised by moderately sorted packstone to grainstone in cuneiform beds with thickness ranging from 20 to 100 cm thick and 100/150 m wide (Figures 6a, 7). Internally, the beds show a low angle planar cross-stratification, locally amalgamated by bioturbation (BI 2–3), consisting of vertical traces of *Thalassainoides* and subordinately by *Ophiomorpha*. Besides benthic foraminifers including miliolids, rotaliids, *Neoconoribina*, *Ammonia*, *Elphidium*, *Lobatula* and *Amphistegina*, the skeletal components are represented by abundant rounded coralline algal fragments and skeletal debris (Figure 6b), mainly represented by echinoids, bivalves and serpulid fragments (*Ditrupa*).

4.2.3.1 | Interpretation. This facies, organised in bioclastic wedges, can be interpreted as the result of shedding of bioclastic sediments produced by seagrass on a vegetated substrate, as well as from nearby productive areas within the euphotic zone carbonate factory. This interpretation is consistent with the foraminiferal assemblage, which is dominated by epiphytic foraminifers such as *Neoconoribina*, *Elphidium* and *Lobatula*. Deposition likely occurred on a wave-dominated ramp between the inner and the middle ramp environments.

Wave and storm activity mixed, fragmented and abraded skeletal debris on mobile substrates. The dispersal of bioclastic grains was primarily driven by storm-induced downwelling flows. No sedimentary structures indicative of longshore transport were observed. The allochthonous nature of the faunal elements is supported by physical structures reflecting high-energy traction flows from the inner to the middle ramp, and by the pervasive laminated to bioturbated texture of the beds (c.f. Massari and D'Alessandro 2012).

4.2.4 | F4 Bioturbated Foraminiferal Packstone to Wackestone

Moderately sorted, fine-grained skeletal packstone to wackestone forms massive beds, up to 2 m thick, with weak traces of planar lamination and abundant bioturbation. Skeletal components are planktonic foraminifers (globigerinids, globigerinoids and globorotalids) and minor benthic foraminifers represented

13652117, 2026, 3, Downloaded from https://onlinelibrary.wiley.com/doi/10.1111/bre.70109 by University Di Roma La Sapienza, Wiley Online Library on [05/05/2026]. See the Terms and Conditions (https://onlinelibrary.wiley.com/terms-and-conditions) on Wiley Online Library for rules of use; OA articles are governed by the applicable Creative Commons License

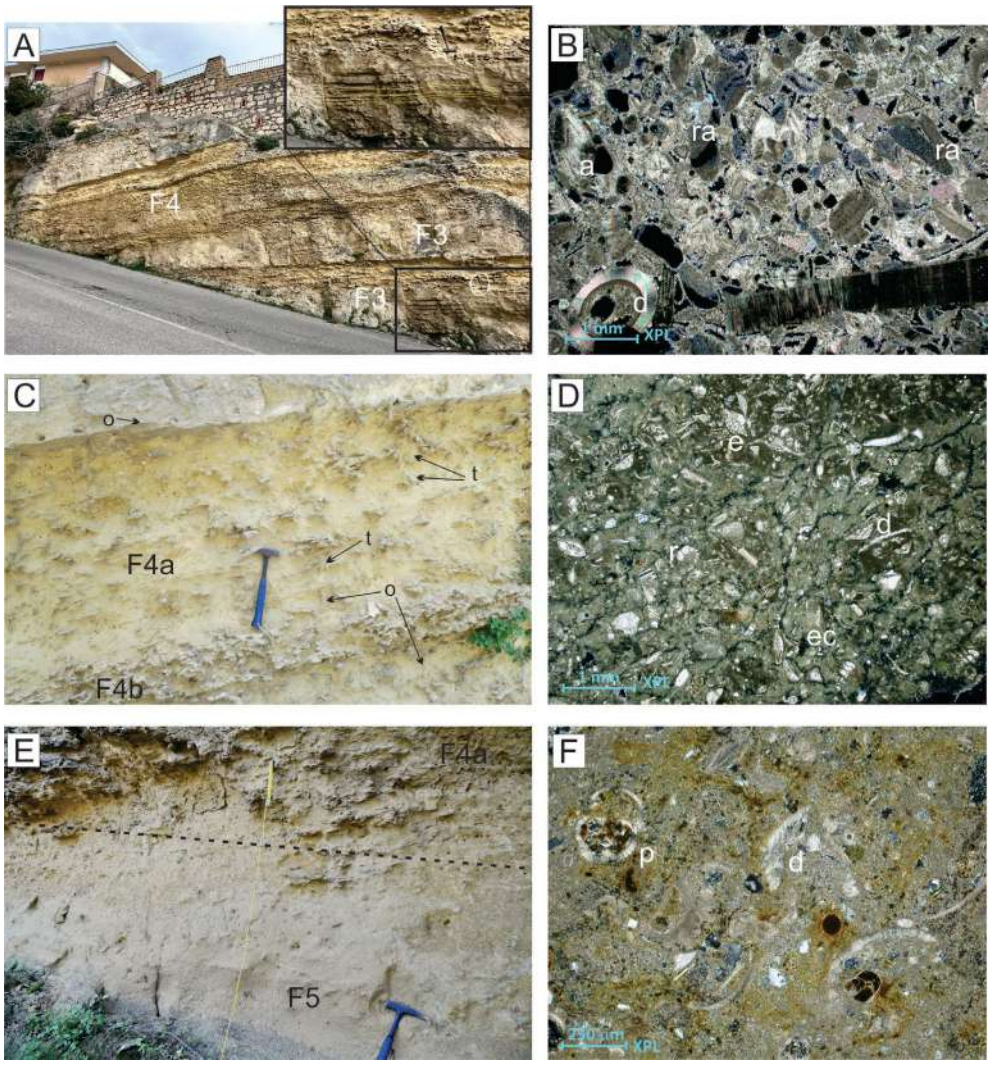


FIGURE 6 | (A, C) Facies F3 Bioclastic packstone to grainstone, (A) This facies is composed of cuneiform beds ranging from 20 to 100 cm in thickness and 100 to 150 m in width. It displays low-angle planar cross-stratification, locally amalgamated due to bioturbation (BI 2–3), primarily featuring vertical burrows of *Thalassinoides*, with subordinate occurrences of *Ophiomorpha* (o); (B) The skeletal components include rounded fragments of coralline algae (ra) and skeletal debris and serpulids (*Ditrupa*, *d*). Benthic foraminifers are also present, including Rotaliids and *Amphistegina* (a). (C, D) Facies F4 Bioturbated Foraminiferal packstone to wackestone. (C) This facies can be subdivided based on bioturbation patterns: F4a subfacies, is slightly coarser-grained and grain-supported, this subfacies shows intense bioturbation (BI 4–5), the dominant ichnogenera include *Thalassinoides* (t) and subordinate vertical *Ophiomorpha* burrows (o); the F4 b subfacies is matrix-supported and intensely bioturbated (BI 6). It typically forms well-cemented, tabular beds ranging from 20 to 50 cm in thickness; (D) the skeletal components include planktonic foraminifers and minor benthic forms such as Discorbids (d), along with occasional *Elphidium* (e). (E) Facies F5 bioclastic mudrock. (E) This facies is characterised by yellowish, fine-grained bioclastic mudrock forming homogeneous beds up to 2 m thick. It exhibits a coarsening-upward trend, with nodular concretions and increasing bioturbation intensity towards the top (BI 4); (F) The bioclastic component is dominated by fine skeletal debris. Identifiable elements include planktonic foraminifers (p) and small benthic foraminifers (*Discorbids*, d).

mainly by buliminids, bolivinids, cibicids and discorbids, with subordinate specimens of *Elphidium*, *Ammonia*, *Lenticulina* (Figure 6d). Ostracods, echinoids, molluscs, bryozoans and *Ditrupa* fragments are rare, as red algal debris. The fine fraction, generally abundant, consists of calcisiltite. Disarticulated bivalve shell lags are common and represented mainly by pectinids. Balanid rhodoids (*sensu* Hottinger 1983) are occasionally present. The siliciclastic fraction is subordinate and shows fine- to medium sand-sized, composed mainly of quartz and more rarely by feldspars and micas. Two main subfacies can be distinguished based on the distribution of bioturbation traces. The F4a subfacies has a slightly coarser grain size and grain-supported texture, tabular beds up to 2.5 m thick. It is characterised by abundant bioturbation (BI 4–5) and is dominated by two main ichnogenera, *Thalassainoides* and subordinate *Ophiomorpha* (Figure 6c,e). The *Thalassainoides* tracks are mainly horizontal, but vertical tracks are also common. The *Ophiomorpha* burrows are vertical only. The texture of F4b is generally matrix-supported and intensely bioturbated (BI 6) with mainly horizontally oriented traces of *Thalassainoides* (Figures 6c, 7). Generally, the F4 b forms well-cemented tabular beds with ranging in thickness from 20 to 50 cm.

13652117, 2026, 3, Downloaded from https://onlinelibrary.wiley.com/doi/10.1111/bre.70109 by University Di Roma La Sapienza, Wiley Online Library on [05/05/2026]. See the Terms and Conditions (https://onlinelibrary.wiley.com/terms-and-conditions) on Wiley Online Library for rules of use; OA articles are governed by the applicable Creative Commons License



FIGURE 7 | Detail of bioturbation in the facies F3 and F4. The F3 is characterised by vertical *Ophiomopha* (o) traces, while the Facies F4b is dominated by horizontal traced of *Thalassinoides* (t).

4.2.4.1 | **Interpretation.** The textural (from grain-supported to matrix-supported) and compositional characteristics of the F4 point (planktonic sediment epiphytic foraminifers, together with pectinids and balanids) point towards sedimentation in a low to moderate energy environment, mostly around the wave base in oxygenated bottom waters between the inner and the middle ramp (c.f. Nalin et al. 2010; Ghinassi 2007; Massari and D'Alessandro 2010). The parautochthonous skeletal particles and terrigenous granules are transported during rare storm events that also produced the shell concentrations. The ichno attributes are consistent with deposition in a relatively quiet depositional environment influenced by oxygenated bottom waters. In particular, *Ophiomorpha*, with its significant vertical shafts, belongs to the *Skolithos* Ichnofacies, but overlaps with the *Cruziana* Ichnofacies, where the horizontal burrowing elements are more pronounced, and where *Thalassinoides* is a common constituent (Figure 7). Furthermore, *Thalassinoides* is often associated with firm substrates. The ichnofacies and textural characteristics of the F4 subfacies suggest a more proximal deposition for the F4a characterised by the presence of *Ophiomorpha* and grain-supported textures and more distal and decreasing sedimentation rate for the F4b characterised by matrix-supported texture, combined with enhanced bioturbation intensity by *Thalassinoides* and cementation, this last associated only with an increase of burrows, promoting the development of a firm bottom.

4.2.5 | F5 Bioclastic Mudrock

This facies consists of yellowish bioclastic mudrock (Figure 6e). The bioclastic fraction is primarily composed of fine skeletal debris, with identifiable components including planktonic foraminifers (globigerinids, globigerinoids, globorotalids) and small benthic foraminifers, mainly Buliminids, bolivinids, cibicids, *Lenticulina* and discorbids (Figure 6f). Rare fragmented *Elphidium*, as well as *Lobatula* and *Amphistegina* tests, have also been observed. Disarticulated bivalve shell lags are common, along with well-preserved infaunal bivalves and occasional *Ditrupa* and irregular echinoids. The terrigenous fraction consists of silt- to sand-sized quartz and mica grains, with glauconitic grains being abundant. This facies has a homogeneous appearance, forming beds up to 2 m thick (Figure 6e), characterised by a coarsening-upward trend, nodular concretions and increasing bioturbation (BI 4) towards the top. Faint traces of hummocky cross-stratification can be observed in the beds.

4.2.5.1 | **Interpretation.** The lack of sedimentary structures, combined with the abundance of planktonic foraminifers, suggests deposition in an environment with moderate to low sedimentation rates, just below or near the storm wave base, as indicated by faint traces of hummocky cross-stratification (HCS) and bivalve lags. The common occurrence of glauconite aligns with low sedimentation rates. The foraminiferal assemblage exhibits moderate mixing of ecologically incompatible forms such as *Amphistegina* and planktonic foraminifers, implying a degree of reworking and redeposition in a middle to outer ramp setting.

4.3 | Stratigraphic Architecture

The physical correlation of the measured stratigraphic sections, along with the panoramic views of the outcrops, reveals that the 'Macco' unit comprises three stacked clino-stratified carbonate prograding wedges (Figure 8).

The foreset of the first and third units is composed of facies F1a, while the second unit transitions from facies F1a to facies F1b on the foreset slope (Figure 8). At the transition to toesets and bottomsets, the foresets are tangentially based. The bottomsets of all three units consist of facies F4, intercalated with bioclastic sands of facies F3 (Figure 6A). Facies F1c is restricted to fault-controlled channels (see Section 4.6).

The second and third prograding units are separated by a 2-m-thick interval of facies F5, which records a transgressive event between the two units. Finally, in the Tomba degli Scudi area, facies F1 laterally interfingers with the Hybrid arenite facies (F2).

4.4 | Biostratigraphy

Each of the analysed samples (PG1, DX12P, DX11P, TXGA, TX10) shows distinct planktonic foraminiferal assemblages, primarily varying in preservation and abundance. Only sample PG1 is very rich in planktonic foraminifera.

4.4.1 | *Globorotalia bononiensis* Subzone (MPl5a, Piacenzian)

Samples PG1, DX11P, DX12P and TX10 are assigned to the *Globorotalia bononiensis* subzone (MPl5a) of the Piacenzian, following the Mediterranean planktonic foraminiferal biozonation of Lirer et al. (2019), although with different levels of confidence depending on assemblage richness and preservation.

Sample PG1 yields a rich, well-diversified and well-preserved planktonic foraminiferal assemblage. The most abundant

13652117, 2026, 3, Downloaded from https://onlinelibrary.wiley.com/doi/10.1111/bre.70109 by University Di Roma La Sapienza, Wiley Online Library on [05/05/2026]. See the Terms and Conditions (https://onlinelibrary.wiley.com/terms-and-conditions) on Wiley Online Library for rules of use; OA articles are governed by the applicable Creative Commons License



FIGURE 8 | Panoramic view of the outcrops showing three clino-stratified, carbonate prograding wedges. The tops and foreset slopes of the first and third wedges are composed of Facies F1a, while the foreset slope of the second wedge shows a transition from Facies F1a to Facies F1b. Two main clinoform sets: (1) a lower set of climbing to prograding clinoforms, downlapping at low dip angles and bounded above by an unconformity; and (2) an upper set characterised by higher dip angles, prograding downslope onto an internal downlap surface evidenced by orange terminations. The overall stacking pattern records progressive infilling of accommodation during a sea-level stillstand (light blue triangle), followed by reduced accommodation associated with relative sea-level fall (orange triangle). Individual prograding wedges are separated by transgressive deposits (facies F5) formed during subsequent sea-level rise and separating the second and third clinostratified prograding wedge.

taxa are *Globigerinoides quadrilobatus*, *Globorotalia crassaformis* and *Orbulina* spp.; *Globigerinoides obliquus obliquus* is common, whereas *G. ruber*, *Globigerinella siphonifera*, and *Globigerina bulloides* are few. *Pulleniatina bulloides* is rare; *Neogloboquadrina pachyderma* (right-coiled) is very rare, and *Globorotalia bononiensis* is present but scarce. The high abundance of *G. crassaformis* coupled with the rarity of *G. bononiensis*, together with the absence of *Neogloboquadrina atlantica atlantica*, *Sphaeroidinellopsis* spp. and *Dentoglobigerina altispira*, and the high frequency of *G. obliquus obliquus*, allows this sample to be placed in the lower part of the MPl5a subzone, between ca. 2.85 and 2.75 Ma.

Samples DX11P and DX12P contain poor and poorly preserved planktonic foraminiferal assemblages. Both are characterised by the presence of *Globorotalia crassaformis* (few), *Globigerina bulloides* and *Orbulina* spp. (rare), *Globigerinoides quadrilobatus* (rare) and *G. ruber* (white morphotype; few); *G. obliquus obliquus* is additionally recorded as rare in DX11P. Despite the absence of *G. bononiensis*, the occurrence of *G. crassaformis* supports assignment to the *G. bononiensis* subzone (MPI5a).

Sample TX10 yields extremely scarce planktonic foraminifera, limited to *G. crassaformis*, *G. obliquus obliquus* and *G. quadrilobatus*. Owing to the very low abundance of diagnostic taxa, its attribution to the MPl5a subzone remains tentative, based solely on the presence of *G. crassaformis*. Sample TXGA is barren.

4.4.2 | Calcareous Nannofossils—MNN15 Zone (Latest Zanclean–Piacenzian)

Samples PG1, DX11P and DX12P yielded calcareous nannofossil assemblages ranging from abundant to rare, with moderate to poor preservation and frequent reworked specimens. All three samples can be assigned, with varying degrees of confidence, to the MNN15 Zone of Di Stefano et al. (2023).

Sample PG1 contains an abundant and well-diversified assemblage dominated by small to medium-sized *Reticulofenestra* spp. *Calcidiscus leptoporus* and *Geminilithella rotula* are common; *Calcidiscus macintyrei*, *Helicosphaera carteri* and *Pseudoemiliania lacunosa* are few. *Helicosphaera sellii*, *Discoaster tamalis*, *D. asymmetricus* and small *Gephyrocapsa* are rare, whereas *Reticulofenestra pseudoumbilicus* and *Sphenolithus* spp. are very rare. The co-occurrence of *D. tamalis*, *P. lacunosa* and small *Gephyrocapsa* allows attribution to the MNN15 Zone, between the Top of *Sphenolithus* spp. and the Top of *Discoaster tamalis*.

Sample DX11P yields common but poorly preserved calcareous nannofossils, dominated by small to medium-sized *Reticulofenestra* spp. *Calcidiscus leptoporus* is common, whereas *Geminilithella rotula*, *Calcidiscus macintyrei* and *Coccolithus pelagicus* are few. *Pseudoemiliania lacunosa* and small *Gephyrocapsa* are very rare. The genus *Discoaster* is virtually absent, represented only by a single fragment of *D. tamalis*. The absence of *Sphenolithus* spp. and *R. pseudoumbilicus*, together with the presence of *P. lacunosa* and *D. tamalis*, supports a tentative assignment to the MNN15 Zone.

Sample DX12P contains rare and moderately to poorly preserved calcareous nannofossils, with an assemblage similar to that of DX11P. Very rare *Discoaster pentaradiatus*, together with *Pseudoemiliania lacunosa* and small *Gephyrocapsa*, were recorded. As in the other samples, the absence of *Sphenolithus* spp. and *R. pseudoumbilicus*, combined with the occurrence of *P. lacunosa* and *D. pentaradiatus*, suggests a cautious attribution to the MNN15 Zone.

4.5 | Morphostructural and Structural Analysis

The analysis of morphostructural (e.g., fault scarps, structural valleys) and structural elements (e.g., bedding planes, fault planes and fractures) provides a comprehensive view of fault orientations at Tarquinia. The dominance of faults and fractures striking E–W and (N)NW across multiple stops is evident in both rose diagrams (Figure 9a,b). The most prominent morphostructural segments broadly strike NW–SE and E–W, while minor structures trend NE–SW. The longest structure bordering the Tarquinia Horst to the southwest has an NW–SE strike and a

13652117, 2026, 3, Downloaded from https://onlinelibrary.wiley.com/doi/10.1111/bre.70109 by University Di Roma La Sapienza, Wiley Online Library on [05/05/2026]. See the Terms and Conditions (https://onlinelibrary.wiley.com/terms-and-conditions) on Wiley Online Library for rules of use; OA articles are governed by the applicable Creative Commons License

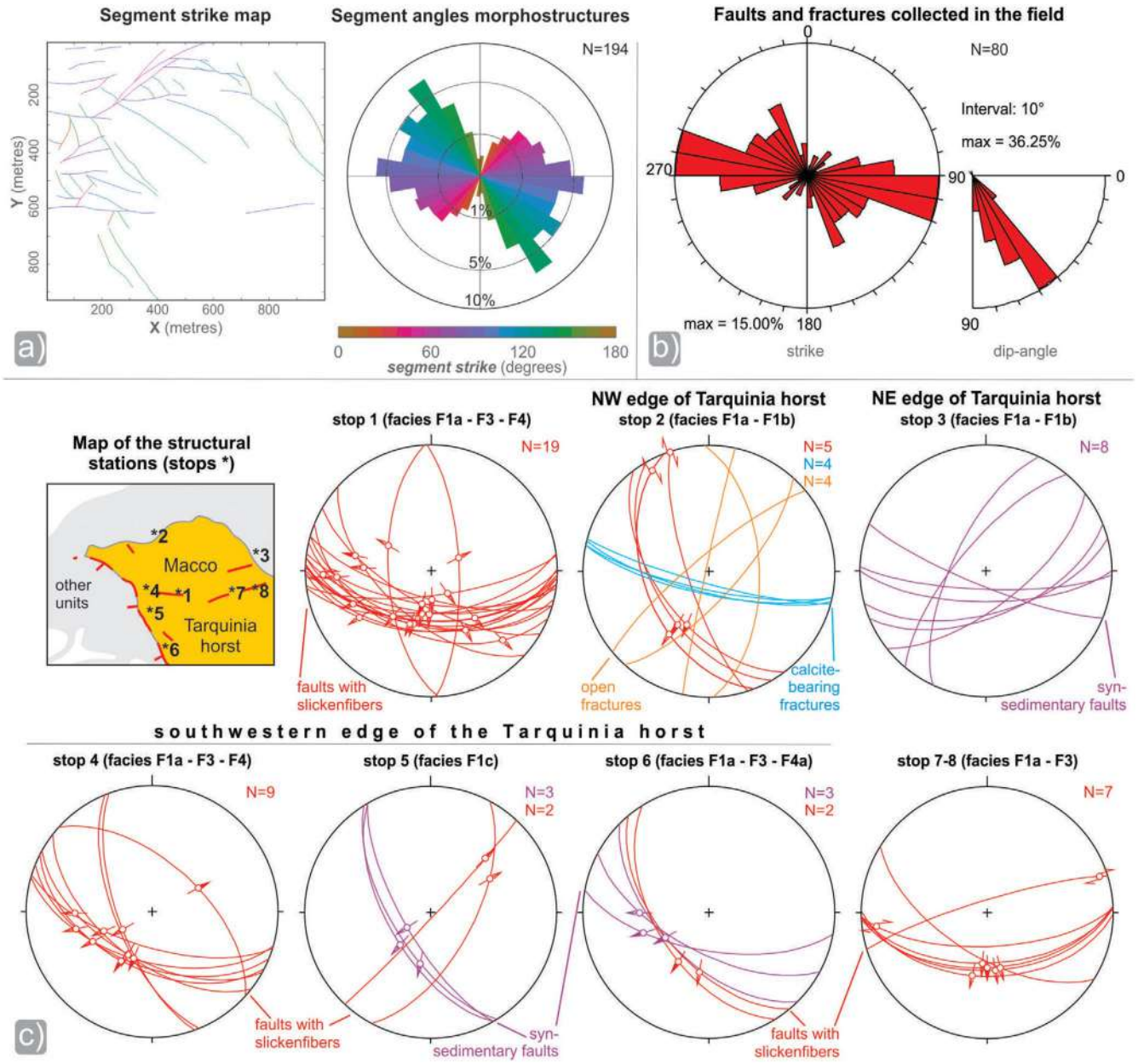


FIGURE 9 | Results of geometric analysis of morphostructures and faults from the geological map and structural stations (stops) are presented in the geological map and at the structural stations (stops). (A) A segment strike map of lineaments and a relative rose diagram, created using FracPaq2, are shown. (B) A rose diagram summarising the strike and dip angle of the faults and fractures collected in the field is presented. E–W and NW-striking features notably dominate both rose diagrams. (C) Stereographic projections (lower hemisphere, Schmidt net) provide detailed fault-plane orientations and kinematic data from eight field stops. Faults with slickenfibers and syn-sedimentary faults tend to strike from WNW to NW along the southwestern edge of the Tarquinia horst.

length of about 3–4 km and displays an overall downstep towards the southwest (Figure 4). This makes it a first-order lineament. Other lineaments, though segmented, have a total length of up to 0.5 km, classifying them as second-order. Field-measured faults share similar strike trends. This indicates significant tectonic influence along the morphostructures. The dip angle of most faults is approximately 50°–70°. These structures also include faults bearing syn-sedimentary features associated with peculiar facies, displaying different geometries and kinematics in different areas. The investigated structural stops exhibit a structural setting including fault systems with slickensides, syn-sedimentary faults and calcite-bearing fractures (see Figure 9).

The stereographic projections provide detailed fault-plane orientations and kinematic data from eight field stops (see Figure 9c).

Each plot visualises the planes of fault and fracture surfaces, along with fault-slip indicators where applicable.

Overall, we recognise that E-W and WNW-ESE trending faults share oblique normal fault kinematics. Stops 1, 7 and 8 represent WNW-ESE striking faults that cut through the Tarquinia horst (see the positional map in Figure 9c), and stops 2 and 3 represent the north-western and north-eastern edges of the horst, respectively. Stops 4, 5 and 6 represent the south-western edge, which

13652117, 2026, 3, Downloaded from https://onlinelibrary.wiley.com/doi/10.1111/bre.70109 by University Di Roma La Sapienza, Wiley Online Library on [05/05/2026]. See the Terms and Conditions (https://onlinelibrary.wiley.com/terms-and-conditions) on Wiley Online Library for rules of use; OA articles are governed by the applicable Creative Commons License

has transtensive faults striking northwest and northeast. Some of these clearly exhibit syn-sedimentary geometries. These faults align roughly parallel to the south-western edge of the Tarquinia horst, while the other two edges have structures that appear not aligned with the south-western fault strike edging the horst. Overall slickensides are almost always faint to absent in the F4 facies but are better preserved in the F3 lithofacies. Calcite-bearing fractures (cyan lines in the stereographic projections of Figure 9) are typically found in the WNW–ESE steepest faults, suggesting post-faulting mineral infill. Open fractures are N–S and NE–SW oriented (orange lines) and do not virtually present significant displacement or mineralisation.

Depending on the location, faults may show evidence of syn-tectonic sedimentary structures, usually indicated by the presence of a bed-sealing termination of the fault towards the top and growth structures (Figure 10a–c). This is well visible in minor structures as well, regardless of their orientation. Sedimentary structures such as dunes (F1b) and channels occur on top of graben-like structures of different dimensions that can be associated with (N)NW–(S)SE striking faults or to NE–SW to E–W striking faults (Figure 10a–c). As depicted in Figure 10b, a forced channel is made by a thicker succession towards NW. Major unconformities are marked by thicker lines, while strata show lateral foresets and thickness variations. A net angular unconformity occurs at the base of the syn-sedimentary succession, marked by an orange dotted line. We observed a few meter-long faults with variable dip angles cutting across facies F1a and F1b between the unconformities, which represent small collapse structures within the succession on the hanging wall of a NE–SW striking fault, whose accessory structures are nearly E-W trending. Regarding the facies associated with the first-order, NW–SE striking fault bordering the southwest of the Tarquinia area in the calcareous beds, the following are present: F1a, F1c, F3 and F4a (Figure 9, stops 4–6). Minor fault steps are also associated with WNW-trending faults. As shown by the red arrows in the line drawing in Figure 10a–c, all lithofacies F1a and F1b are cut by high-angle faults with displacements ranging from 1 to 0.1 m, although a more gentle dip angle is observed in marly intercalations, as well as termination of displacement and change of fault orientation. We observed a few meter-long faults with variable dip angles cutting across facies F1a and F1b between the unconformities.

As shown in the NE sector of the Tarquinia area in Figure 10b,c, thus, a major growth wedge is observed against a minor NE–SW trending fault, with a thicker succession towards the NW in facies F1b with faults affecting the whole unit. At Stop 5, a shear zone approximately two meters thick has been observed. This shear zone occurs in the footwall and has low-angle shear planes with the bedding. The broad shear zone has also been observed in F3 facies (Figure 10d), and it is associated with a NW-striking channel (Figure 10d) that can be interpreted as a fault-forced channel. The hanging wall block hosts a damaged zone of high-angle faults with displacements averaging a few centimetres.

Minor faults were mapped along the first order NW-SE fault. Figure 11, shows field examples of these faults, as seen at Stop 6. Locally WNW- and NW-striking faults with offset ranging a few decimetres are characterised by oblique normal faults associated with beds that seal the faults. These are the typical structures of syn-sedimentary structure affecting facies F1a.

As shown in Figure 11a, beds also down-step towards the North along antithetic minor faults. At the transition with the marly facies, faults are observed in the most competent layers of facies F3 that are connected in the marly layers of facies F4a by dilation bands (Figure 11). As exemplified in Figure 10c, these dilation bands resemble brittle-ductile structures in Facies F3, probably due to the syn-sedimentary transtensional activity within quite soft sediments (F4a) and poorly cemented lithofacies F3.

5 | Discussion

5.1 | Syn-Sedimentary Tectonics

The interpreted depositional model takes into account the regional tectonic framework and the field evidence reported for the Tarquinia area, which confirms the existence of syn-sedimentary faulting during the Late Pliocene, also documented further southeast by Balsamo et al. (2008). The fault system bounding the NW-trending Tarquinia basin to the southwest (Figures 2, 4) consists of a few kilometres long NW–SE striking fault segments that controlled the formation of growth structures and determined glidings and sediment deformation (Figure 10d). Line drawings of faults and bedding geometries in the northeastern and northwestern areas of Tarquinia further support the presence of first order NW-striking faults and smaller NE- and E–W striking syn-sedimentary oblique normal fault structures (Figures 4, 9). These second order faults forced the formation of channels and dunes (Section 4.5).

5.2 | Depositional Model and Paleonvironments

Plio-Pleistocene shallow-water carbonate deposits in the Mediterranean region formed within small, high-gradient ramp settings. Their stratigraphic architecture was primarily controlled by high-amplitude, orbitally driven glacio-eustatic fluctuations, often recorded through repeated progradational episodes (e.g., Chiocci and Orlando 1996; Catalano et al. 1998; Read 1998; Vitale 1998; Pomar and Tropeano 2001; Massari et al. 2002; Roveri and Taviani 2003; Massari and Chiocci 2006; Massari and D'Alessandro 2012; Chiarella et al. 2012, 2019; Chiarella and Longhitano 2012).

The Pliocene–Pleistocene coastal systems and carbonate ramps documented in the sedimentary succession of the Apennines, Sicily and Spain show many analogies with the facies belt of these depositional systems in the most tectonically active systems of the modern Mediterranean (MartÍn et al. 2004; Ghinassi 2007; Nalin et al. 2010, 2016; Massari and D'Alessandro 2012). As the local syn-sedimentary tectonics is most strongly developed along the first-order fault intersecting the ramp to the southwest, this structure likely generated accommodation space in that direction, while exerting only minor control on the SW–NE-oriented structures. In this context, second-order faults played an important role in the formation of fault-controlled dunes and channels on which the dunes' travel or transport velocity changed. During their development, these grabens may

13652117, 2026, 3, Downloaded from https://onlinelibrary.wiley.com/doi/10.1111/bre.70109 by University Di Roma La Sapienza, Wiley Online Library on [05/05/2026]. See the Terms and Conditions (https://onlinelibrary.wiley.com/terms-and-conditions) on Wiley Online Library for rules of use; OA articles are governed by the applicable Creative Commons License

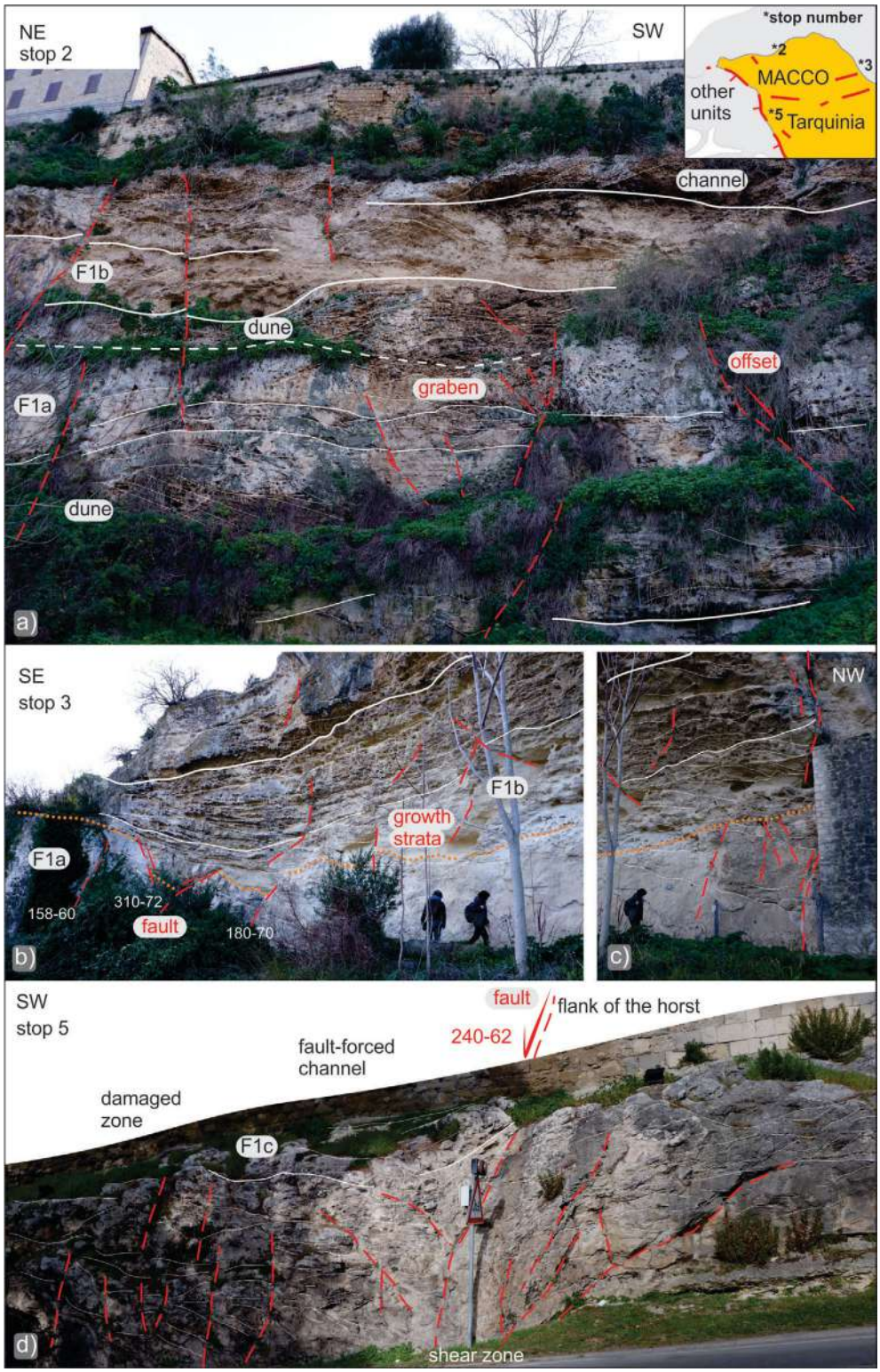


FIGURE 10 | Syn-sedimentary evidence in the 'Macco' unit. (a) Stratigraphic succession (42°15′23.13″ N, 11°45′12.57″ E) with high-angle faults with displacements less than 1 m cut through all lithofacies. Major unconformities are marked with thicker lines. Strata show lateral foresets and thickness variations due to horst-and-graben faults. (b, c), a major growth wedge is observed against a NE–SW trending fault, with thicker successions towards the NW in facies F1b (42°15′14.87″ N 11°45′43.06″ E). Fault displacements range from 1 m at the base to 0.01 m at the top. An angular unconformity at the base of the syn-sedimentary succession is marked by an orange dotted line. (d) fault-forced channel at the hanging wall of a shear zone with low-angle shear planes edging the horst (42°15′3.57″ N 11°45′16.33″ E). Near the contact between the competent F3 layers and the bioturbated marly layers, dilation bands and fault offsets occur.

13652117, 2026, 3, Downloaded from https://onlinelibrary.wiley.com/doi/10.1111/bre.70109 by University Di Roma La Sapienza, Wiley Online Library on [05/05/2026]. See the Terms and Conditions (https://onlinelibrary.wiley.com/terms-and-conditions) on Wiley Online Library for rules of use; OA articles are governed by the applicable Creative Commons License



FIGURE 11 | Syn-sedimentary evidence within 'Macco' facies (42°14′58″ N, 11°45′20″ E). (a) Onlap structures are observed on soft-sediment deformed calcarenitic beds. Bricks are a human-made construction within a karstified carved 'Macco' unit at a road cut. (b) At the transition with the marly facies, faults occur in the most competent layers and are connected by dilation bands in the marly layers. (c) Dilation bands within calcarenites, offsetting the limit with poorly cemented bioturbated Foraminiferal packstone to wackestone (F4).

have caused local collapses that produced the coarser and more chaotic facies F1c that resemble conglomerates. The recorded syn-sedimentary effects of distributed faulting seem to decrease in intensity towards the top of the succession, corresponding to the latest Pliocene or Early Pleistocene, before the final exposure of the succession during the Early Pleistocene (Bulian, Marra, et al. 2024).

The result of facies analysis shows that the bioclastic carbonate fraction of the 'Macco' unit is generally abundant even if locally

13652117, 2026, 3, Downloaded from https://onlinelibrary.wiley.com/doi/10.1111/bre.70109 by University Di Roma La Sapienza, Wiley Online Library on [05/05/2026]. See the Terms and Conditions (https://onlinelibrary.wiley.com/terms-and-conditions) on Wiley Online Library for rules of use; OA articles are governed by the applicable Creative Commons License

the terrigenous input can be conspicuous up to 50%. Taking into account the depositional profile that can be obtained with the stratigraphic section correlation, it can be ascribed to a mixed siliciclastic-carbonate distally steepened carbonate ramp (c.f. Massari and D'Alessandro 2010).

In the inner ramp the sandy and gravelly substrates are colonised by seagrass meadows that host a significative carbonate production operated by epiphytic biota, (mainly foraminifers and coralline algae) and biota living on the substrate such as echinoids, bivalves, gastropods (Mateu-Vicens et al. 2012; Gaglianone et al. 2017; Brandano et al. 2019). In the Mediterranean these environments are made of siliciclastic-carbonate mixing (Fornos and Ahr 1997; Betzler et al. 1997; Brandano and Civitelli 2007; Mateu-Vicens et al. 2012; Brandano et al. 2019). The terrigenous fraction is sourced by fluvial input and coastal erosional processes (c.f. Mount 1984; Halfar et al. 2004; Brandano and Civitelli 2007), while the carbonate fraction mainly derives by carbonate biota producing sediment that live in the substrate and on the leaves of seagrass meadows (Betzler et al. 1997; Mateu-Vicens et al. 2012; Brandano et al. 2019). In the middle ramp, the seafloor is dominated by carbonate sediment (Carannante et al. 1988; Fornos and Ahr 1997; Betzler et al. 1997; Brandano and Civitelli 2007; Aguirre et al. 2012). In this case the main biota producing carbonate are the coralline algae developing in the oligophotic zone. Coralline algae are present in two main growth forms depending by hydrodynamic conditions and the associated fauna (Marrack 1999; Nalin et al. 2010; Basso et al. 2017), as free living branches, forming the well-known facies of mäerl in low energy settings (Basso et al. 2008, 2017), and as rhodoliths in low to high energy conditions. The larger benthic foraminifer *Amphistegina* is abundant in this environment forming local accumulations (Di Bella et al. 2005) in association with an abundant mollusc fauna (Coletti et al. 2021). Basinward of the middle ramp deposits, the dip of bedding planes increases to 15°–20°, with sediment predominantly composed of coralline algae in the form of rhodoliths and free-living branches. The progressive steepening of the slope towards the basin indicates an area of increased sedimentation, resulting from the combined accumulation of in situ gravel-sized skeletal components produced in the oligophotic zone and skeletal debris transported downslope from shallower areas (e.g., Pomar et al. 2002). The lower slope and its transition to the outer ramp are characterised by normal grading and pervasive planar lamination, often obscured by extensive bioturbation (Figure 7). As noted by several authors (e.g., Quiquerez and Dromart 2006; Massari and D'Alessandro 2012), offshore-directed, storm-induced traction flows transitioned into sediment gravity flows, with dense suspensions moving beyond the slope break and being transported downslope. The shift from laminated to bioturbated bedding reflects the peak and waning stages of high-energy events, followed by intense recolonisation of the seafloor by benthic organisms. Further basinward (i.e., towards the SW), the ramp slope transitions into the outer ramp, where carbonate production decreases and is dominated by aphotic biota. Carbonate sedimentation in this setting is mainly driven by small benthic and planktonic foraminifers, regular and irregular echinoids and filter-feeding fauna such as molluscs and bryozoans, along with contributions from siliceous organisms, including siliceous sponges. The outer ramp is marked by a significant increase of clay content and represented in this case by the Pian della Regina lithostratigraphic unit.

The depositional profile is the result of the *loci* of carbonate production, the inherited substrate and the type of accommodation (Pomar 2001). In a setting dominated by physical accommodation (sensu Pomar 2001), the depth of sediment accumulation is controlled by storm wave base and storm-driven flows and defines a shelf surface of dynamic equilibrium between sediment supply and removal (Swift and Thorne 1991; Pomar 2001; Pomar and Kendall 2008). The investigated ramp is predominantly shaped by the dispersal of bioclastic sediments, largely controlled by storm-driven downwelling flows. These include offshore-flowing near-bottom return currents that counterbalanced the onshore displacement of water caused by storm-driven winds (cf. Chiocci and Orlando 1996; Pomar and Tropeano 2001; Pomar and Kendall 2008). Storm events transported bioclastic sediment basinward, depositing it on the ramp slope, where clinobeds represent the main locus of accumulation and preservation of skeletal material. This selective transport process effectively bypassed fine-grained particles, including silt, clay, and the limited carbonate mud produced by bioerosion and mechanical abrasion. As a result, fine-grained sediments were primarily incorporated and accumulated in offshore or outer ramp mud deposits. Similar systems lacking the fine-grained fraction have been investigated in the Plio-Plestocene of Southern Apennines (e.g., Pomar and Tropeano 2001; Chiarella et al. 2012; Chiarella and Longhitano 2012).

5.3 | Carbonate-Siliciclastic Mixing

Carbonate-siliciclastic mixing primarily occurs in the innermost environments of the inner ramp due to coastal erosional processes and episodic fluvial inputs (e.g., Mount 1984; Brandano and Civitelli 2007; Chiarella et al. 2012, 2017; Chiarella and Longhitano 2012; Tomassetti and Brandano 2013; Zecchin 2017; Schwarz et al. 2018). More structured fluvial systems can give rise to well-developed delta systems, which supply sand bedforms reworked by storm-induced currents that intercalate with the bioclastic deposits of the middle ramp. In the studied case, these terrigenous sands derive from emergent areas along the shoreline and are subsequently redistributed across the shallow sectors of the ramp, where they interfinger with red algal floatstone to rudstone facies under high-energy conditions. These energetic processes are likely driven by a combination of storm and waves. During storms, the combined effects of waves and winds generate offshore-directed currents, which transport sediment towards the shelf (Wright et al. 1991; Héquette et al. 2001; Gil-Gil et al. 2024).

Accordingly, the fine-grained terrigenous component progressively increases towards the basin, whereas the coarser fraction dominates the shallowest environments. Basinward of the seagrass meadows, the skeletal carbonate fraction increases, reaching a maximum in the oligophotic zone dominated by red algae. Farther offshore, the terrigenous input rises again, but is mainly represented by fine-grained silt and clay, which prevail across the outer ramp.

A similar distribution trend can be observed in the modern Pontinian Islands and in the Majorca ramp of Central and Western Mediterranean, where carbonate-siliciclastic mixing begins in seagrass meadows, followed by a pure carbonate factory active in the oligophotic zone, and then transitions to an offshore environment where the terrigenous fraction becomes abundant,

13652117, 2026, 3, Downloaded from https://onlinelibrary.wiley.com/doi/10.1111/bre.70109 by University Di Roma La Sapienza, Wiley Online Library on [05/05/2026]. See the Terms and Conditions (https://onlinelibrary.wiley.com/terms-and-conditions) on Wiley Online Library for rules of use; OA articles are governed by the applicable Creative Commons License

dominated by silt and clay (Carannante et al. 1988; Fornos and Ahr 1997; Brandano and Civitelli 2007; Mateu-Vicens et al. 2012).

5.4 | 'Macco' a Regressive Unit

The facies and architecture of the bioclastic heterozoan dominated ramps are highly sensitive and rapidly responsive to changes in accommodation, as they are in equilibrium with seawater dynamics. As a result, they are predominantly controlled by physical accommodation (after Pomar 2001; Pomar and Kendall 2008; Schlager 2003).

Notably, a relative sea-level fall does not necessarily lead to the shutdown of the carbonate factory. Instead, the system can adapt by migrating seaward, forming a seaward-sloping wedge with an architectural style that closely resembles that of siliciclastic margins (Schlager 2005).

The stratigraphic architecture of 'Macco' is characterised by three stacked clino-stratified carbonate prograding wedges. The quality and exposure of the outcrops allowed for a detailed analysis of the second wedge's architecture. Within this unit, a first set of climbing to prograding clinoforms can be identified, downlapping at low dip angles and separated by an unconformity. Above this surface, a second set of clinoforms shows an increased dip angle, prograding downslope on this surface that corresponds to the internal downlap surface described by Pomar and Tropeano (2001). This stacking pattern is widely interpreted as the progressive infilling of available accommodation space during a sea-level stillstand, followed by a gradual loss of accommodation as sea level fell. The prograding wedges are separated by transgressive deposits, formed during sea-level rise and represented by facies F5.

Similar prograding wedges have been described in the Plio-Plestocene shallow water deposits of the Western Mediterranean, in particular southern Italy, in Sicily (Likorish and Butler 1996; Colella and Vitale 1998; Massari and Chiocci 2006; Massari and D'Alessandro 2010, 2012) and in the Bradanic area, Matera (Pomar and Tropeano 2001), in northern Italy (Roveri and Taviani 2003; Nalin et al. 2016), in the offshore of the Tyrrhenian coast (Chiocci and Orlando 1996; Massari and Chiocci 2006), in SE Spain (MartÍn et al. 2004) and also in the north-east of Rhodes, Greece (Hansen 1999). They are interpreted as brief, rapid episodes of orbitally forced falling stage progradation of distally steepened ramps. Nevertheless, in the present study, the age derived from biostratigraphic analysis enables a correlation with the global eustatic cycles defined by Miller et al. (2020). The base of the 'Macco' calcarenite, and thus the base of the first sedimentary wedge, falls within the *Globorotalia crassaformis* subzone (MPl4b). In contrast, the base of the uppermost wedge is dated between 2.75 and 2.85 Ma. This correlation clearly shows that the three wedges correspond to three major eustatic cycles that occurred during the Piacenzian (Figure 12a,b).

5.5 | The Coralline Algae Carbonate Factory

The skeletal assemblage of the 'Macco' unit primarily falls within the heterozoan category, and the middle ramp carbonate factory is dominated by coralline algae. As highlighted by Aguirre and Braga (2024), coralline algae deposits first appeared in the Early Cretaceous and expanded significantly during the Cenozoic, with notable peaks in the Priabonian and again during the Miocene, particularly in the Aquitanian-Langhian. Following a Langhian maximum, coralline algae deposits experienced a sharp decline, reaching a minimum in the Zanclean period. According to Halfar and Mutti (2005), the general increase in seawater fertility, driven by intensified upwelling currents and increased fluvial discharge as a result of continental weathering after the Mid-Miocene Climatic Optimum (MMCO), played a key role in the development of rhodolith-dominated facies. Similarly, Pomar et al. (2017) suggested a connection between red algae as dominant platform builders and positive excursions of $\delta^{13}C$, reflecting an increase in oceanic trophic resources.

In contrast, Braga (2017) attributed the proliferation of red algae-dominated carbonate factories of the Miocene to palaeogeographical changes in the Mediterranean domain, which facilitated the formation of numerous small islands surrounded by terrigenous-starved shallow platforms under subtropical to warm-temperate conditions. During the Pliocene, moderate sea levels, stable pH, seawater temperature and pCO_2 levels did not adversely affect rhodolith bed deposits. Aguirre and Braga (2024) further linked the Late Miocene–Pliocene reduction in rhodolith-dominated deposits and the so-called Miocene carbonate crash (Torfstein and Steinberg 2020) to these changing conditions (reduced marine carbonate accumulation in pelagic realm). Additionally, a significant increase in terrigenous deposition during the Pliocene has been observed worldwide (Walker et al. 2002), following major orogenic events. This drastic paleogeographic reorganisation, coupled with substantial terrigenous input, likely explains the decline in coralline algae-rich beds during the Late Miocene to Early Pliocene.

The 'Macco' history shows a sudden change in the environmental conditions that promoted the coralline algae carbonate factory that developed using the growth form of free-living branches forming the depositional facies known as *mäerl*. Probably, two main factors drove the establishment of this carbonate factory. The transgression over the underlying lower Pliocene lithostratigraphic unit may have supported the onset of carbonate deposition, and in particular the establishment of the red algae factory by providing new wide substrate within the photic zone and reducing the siliciclastic input through landward confinement. Additionally, a warm climatic event further enhanced the carbonate production by coralline algae. This is in agreement with the climatic reconstruction by Di Bella et al. (2005). These authors, in their study of *Amphistegina*-rich deposits, dated these deposits to between 3.3 and 3.0 Ma, based on the presence of planktonic foraminifera *Globorotalia bononiensis* and *Globorotalia aemiliana*, which indicate warm conditions preceding the first Pliocene climatic deterioration.

These interpretations are consistent with numerous Pliocene examples where rhodoliths deposits are abundant (Dorsey 1997; Johnson et al. 2012; Johnson 2026; Rebelo et al. 2016, 2025). These examples nothwithstanding representative of diverse palaeogeographical settings display a common facies association indicative of carbonate production on hydrodynamically active, carbonate ramps and in mixed carbonate-siliciclastic ramps.

13652117, 2026, 3, Downloaded from https://onlinelibrary.wiley.com/doi/10.1111/bre.70109 by University Di Roma La Sapienza, Wiley Online Library on [05/05/2026]. See the Terms and Conditions (https://onlinelibrary.wiley.com/terms-and-conditions) on Wiley Online Library for rules of use; OA articles are governed by the applicable Creative Commons License

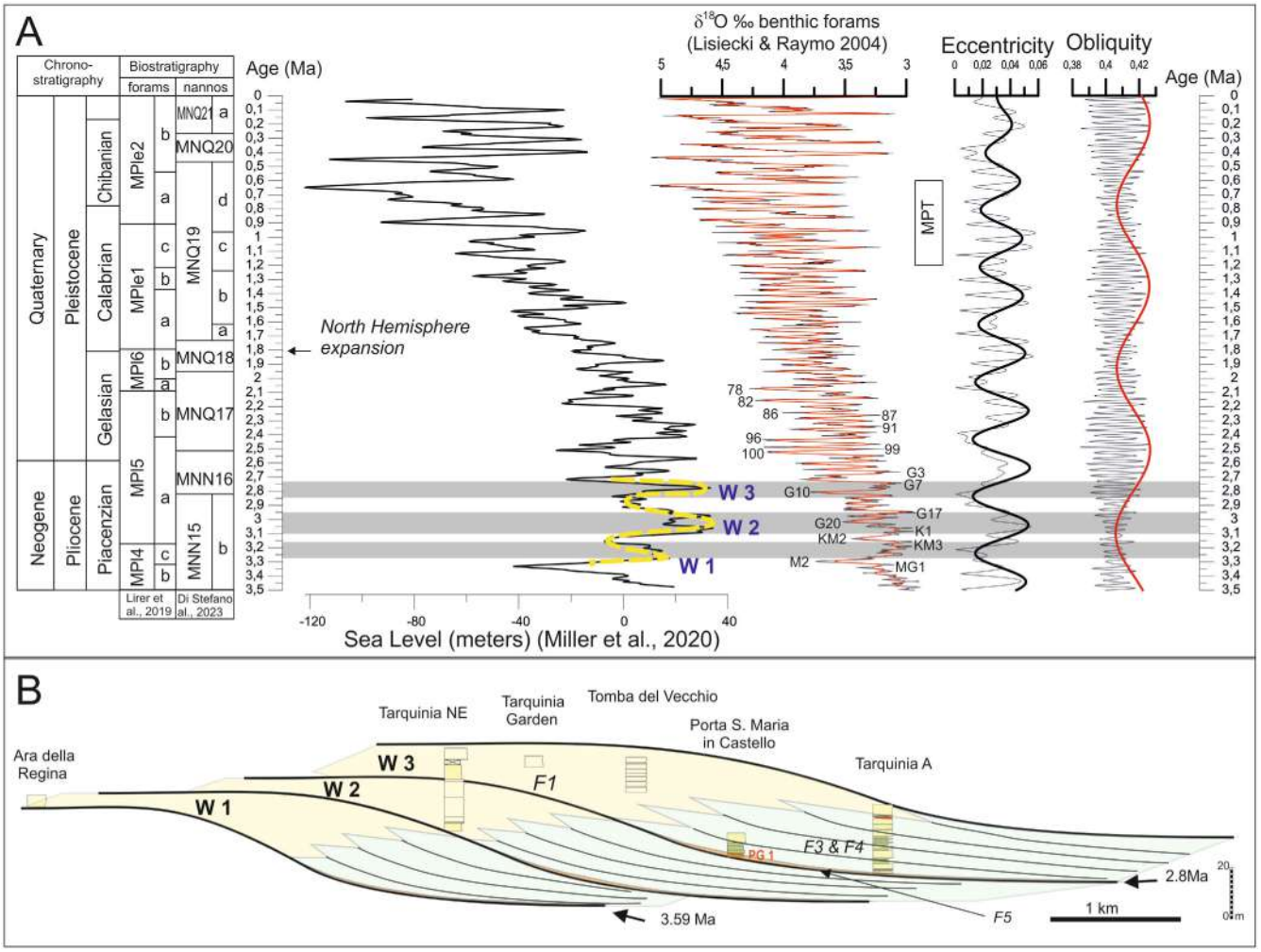


FIGURE 12 | (a) Chronostratigraphic scheme showing the stratigraphic position of the 'Macco' unit and the correlation with the main global eustatic changes by Miller et al. (2020). Planktonic foraminiferal and calcareous nannofossil schemes are from Lirer et al. (2019) and Di Stefano et al. (2023) respectively (b) Schematic stratigraphic architecture with facies association for the 'Macco' unit (For the facies classification see Figure 3).

Rhodolith beds are preferentially developed within transgressive and highstand phases, reflecting intervals of reduced terrigenous input and enhanced accommodation, which favoured coralline algal growth. Rhodolith production and accumulation occurred mainly in middle ramp environments in moderate-energy conditions and limited sediment trapping. Neverthless rhodolith-bearing facies can occur also interbedded with conglomerates and coarse-grained siliciclastics record nearshore to shoreface environments influenced by rocky coastlines, fan-delta systems and fault-controlled margins. In these settings, rhodoliths commonly occur as fragmented or reworked grains within high-energy shoreface environments, indicating episodic transport and redeposition driven by storms, longshore currents and tectonically induced shoreline instability. Finally, local geomorphological barriers (e.g., spits, fan deltas, dikes or volcanic promontories) commonly created leeward, reduced-energy zones, enabling rhodolith accretion even in otherwise energetic coastal systems (Aguirre et al. 2012).

Thus, the simultaneous availability of suitable substrate for the carbonate factory and the climatic conditions supported the proliferation of the coralline algae production even during a time interval when these biota were not typically dominant carbonate producers.

6 | Conclusion

Structural and facies analysis and the morpho-structural analysis in the 'Macco' unit in Tarquinia (central Italy) suggest the presence of Late Pliocene syn-sedimentary structures associated with the deposition of shallow-water sediment in the Tarquinia peri-Tyrrhenian half-graben basins. Overall, syn-sedimentary structures force the distribution of facies including the flow directivity and, thus, shape the Macco wedge. The facies analysis of the 'Macco' lithostratigraphic unit indicates deposition within a mixed siliciclastic-carbonate distally steepened ramp system. In the inner ramp, terrigenous coastal deposits intergrade with seagrass meadows, which significantly contribute to carbonate production. Moving seaward to the middle ramp, carbonate sedimentation is dominated by coralline algae, primarily forming free-living branches with subordinate rhodoliths. The larger benthic foraminifer *Amphistegina* is also abundant in this environment.

13652117, 2026, 3, Downloaded from https://onlinelibrary.wiley.com/doi/10.1111/bre.70109 by University Di Roma La Sapienza, Wiley Online Library on [05/05/2026]. See the Terms and Conditions (https://onlinelibrary.wiley.com/terms-and-conditions) on Wiley Online Library for rules of use; OA articles are governed by the applicable Creative Commons License

The middle ramp exhibits a progressive steepening towards the basin, indicating an increased sedimentation rate. This results from the accumulation of in situ gravel-sized skeletal components, along with material transported downslope from the inner and middle ramp environments. The lower slope and its transition to the outer ramp are characterised by intense bioturbation. In the outer ramp, carbonate production decreases, with aphotic biota dominating and clay content significantly increasing.

The depositional profile of the studied ramp reflects the redistribution of bioclastic sediments, largely controlled by storm-driven downwelling flows. Storm events transported bioclastic material basinward, depositing it along the ramp slope, where clinobeds serve as the primary sites for skeletal material accumulation and preservation.

Carbonate-siliciclastic mixing occurs predominantly in the innermost parts of the inner ramp due to coastal erosion and episodic fluvial inputs. However, mixing also occurs in the middle ramp, where terrigenous sands from emergent areas were reworked by storms and intercalated with red algal floatstone to rudstone facies. In the outer ramp, the terrigenous fraction increases again, though it mainly consists of fine-grained silt and clay.

The facies distribution and architecture of these ramps are highly sensitive to changes in accommodation space. The stratigraphic architecture of the 'Macco' unit consists of three stacked, clinostratified carbonate wedges. The first set of clinoforms exhibits climbing to progradational geometries, downlapping at low dip angles and separated by an unconformity. Above this, a second set of clinoforms with a steeper dip angle prograded downslope. Overall, this stacking pattern reflects progressive infilling of available accommodation space during a sea-level stillstand, followed by a gradual loss of accommodation as sea level fell.

Biostratigraphic analysis indicates that the 'Macco' calcarenite falls in the *Globorotalia crassaformis* Subzone (MPl4b), with the base of the uppermost wedge dated between 2.75 and 2.85 Ma (*G. bononiensis* subzone, MPI5a). Correlation with global eustatic sea-level curves suggests that the development of the three carbonate wedges is closely linked to eustatic fluctuations during the Piacenzian.

The primary carbonate producers in the 'Macco' unit are coralline algae, the dominant constituents of the middle ramp's oligophotic carbonate factory. While coralline algae experienced a significant decline in production and diversification globally after the Middle Miocene—reaching a minimum in the Zanclean—the studied example suggests that warm seawater and an extensive oligophotic carbonate factory along the central Mediterranean coast during the Piacenzian facilitated their continued proliferation.

Acknowledgements

This research was supported by Sapienza University through Ateneo projects. We gratefully acknowledge Mauro Buttinelli and Giuseppe Vico from the National Institute of Geophysics and Volcanology for their valuable discussions, which greatly contributed to our understanding of the subsurface structural setting of the broader study area. The reviewers, Sara Tòmas and Domenico Chiarella, are gratefully acknowledged for their insightful comments and constructive criticism, which led to significant improvements in the manuscript. We also thank Domenico Mannetta for preparing high-quality thin sections and Giovanni Gaglianone for conducting the sedimentological analyses.

Funding

This work was supported by Sapienza Università di Roma.

Conflicts of Interest

The authors declare no conflicts of interest.

Data Availability Statement

The data that support the findings of this study are available from the corresponding author upon reasonable request.

References

Acocella, V., and R. Funiciello. 2006. "Transverse Systems Along the Extensional Tyrrhenian Margin of Central Italy and Their Influence on Volcanism." *Tectonics* 25, no. 2: 1–24. https://doi.org/10.1029/2005TC001845.

Aguirre, J., and J. C. Braga. 2024. "Rhodolith Beds in a Shifting World: A Palaeontological Perspective." *Aquatic Conservation: Marine and Freshwater Ecosystems* 34: e7001. https://doi.org/10.1002/aqc.70015.

Aguirre, J., J. C. Braga, J. M. Martín, and C. Betzler. 2012. "Palaeoenvironmental and Stratigraphic Significance of Pliocene Rhodolith Beds and Coralline Algal Bioconstructions From the Carboneras Basin (SE Spain)." *Geodiversitas* 34, no. 1: 115–136.

Balsamo, F., F. Storti, B. Piovano, F. Salvini, F. Cifelli, and C. Lima. 2008. "Time Dependent Structural Architecture of Subsidiary Fracturing and Stress Pattern in the Tip Region of an Extensional Growth Fault System, Tarquinia Basin, Italy." *Tectonophysics* 454, no. 1–4: 54–69.

Barberi, F., G. Buonasorte, R. Cioni, et al. 1994. "Plio-Pleistocene Geological Evolution of the Geothermal Area of Tuscany and Latium." *Memorie Descrittive Della Carta Geologica D'italia* 49: 77–134.

Bartole, R. 1995. "The North Tyrrhenian–Northern Apennines Post-Collisional System: Constraints for a Geodynamic Model." *Terra Nova* 7, no. 1: 7–30.

Basso, D., L. Babbini, A. A. Ramos-Esplá, and M. Salomidi. 2017. "Mediterranean Rhodolith Beds." In *Rhodolith/Maërl Beds: A Global Perspective. Coastal Research Library*, edited by R. Riosmena-Rodríguez, W. Nelson, and J. Aguirre, vol. 15, 281–298. Springer. https://doi.org/10.1007/978-3-319-29315-8_11.

Basso, D., D. Vrsaljko, and T. Grgasović. 2008. "The Coralline Flora of a Miocene maërl: The Croatian "Litavac"." *Geologia Croatica* 61, no. 2–3: 333–340.

Bernasconi, M. P., and E. Robba. 1993. "Molluscan Palaeoecology and Sedimentological Features: An Integrated Approach From the Miocene Meduna Section, Northern Italy." *Palaeogeography, Palaeoclimatology, Palaeoecology* 100, no. 3: 267–290.

Bernoulli, D. 2001. "Mesozoic-Tertiary Carbonate Platforms, Slopes and Basins of the External Apennines and Sicily." In *Anatomy of an Orogen: The Apennines and Adjacent Mediterranean Basins*, 307–325. Springer Netherlands.

Betzler, C., T. C. Brachert, and J. Nebelsick. 1997. "The Warm Temperate Carbonate Province: A Review of the Facies, Zonations, and Delimitations." *Courier Forschungsinstitut Senckenberg* 201, no. 201: 83–99.

13652117, 2026, 3, Downloaded from https://onlinelibrary.wiley.com/doi/10.1111/bre.70109 by University Di Roma La Sapienza, Wiley Online Library on [05/05/2026]. See the Terms and Conditions (https://onlinelibrary.wiley.com/terms-and-conditions) on Wiley Online Library for rules of use; OA articles are governed by the applicable Creative Commons License

Bown, P. R., J. A. Lees, and J. R. Young. 2004. "Calcareous Nannoplankton Evolution and Diversity Through Time." In *Coccolithophores: From Molecular Processes to Global Impact*, edited by H. R. Thierstein and J. R. Young, 481–508. Berlin.

Braga, J. C. 2017. "Neogene Rhodoliths in the Mediterranean Basins." In *Rhodolith/Maërl Beds: A Global Perspective*, edited by R. Riosmena-Rodríguez, W. Nelson, and J. Aguirre, 169–193. Basel.

Braga, J. C., J. M. Martín, C. Betzler, and J. Aguirre. 2006. "Models of Temperate Carbonate Deposition in Neogene Basins in SE Spain: A Synthesis." *Geological Society, London, Special Publications* 255, no. 1: 121–135.

Branca, S., A. Cinquegrani, R. Cioni, et al. 2023. "The Italian Quaternary Volcanism." *Alpine and Mediterranean Quaternary* 36, no. 2: 221–284. https://doi.org/10.26382/AMQ.2023.09.

Brandano, M., and G. Civitelli. 2007. "Non-Seagrass Meadow Sedimentary Facies of the Pontinian Islands, Tyrrhenian Sea: A Modern Example of Mixed Carbonate–Siliciclastic Sedimentation." *Sedimentary Geology* 201, no. 3–4: 286–301.

Brandano, M., L. Tomassetti, G. Mateu-Vicens, and G. Gaglianone. 2019. "The Seagrass Skeletal Assemblage From Modern to Fossil and From Tropical to Temperate: Insight From Maldivian and Mediterranean Examples." *Sedimentology* 66, no. 6: 2268–2296.

Brogi, A., L. Fabbrini, and D. Liotta. 2011. "Sb–hg Ore Deposit Distribution Controlled by Brittle Structures: The Case of the Selvena Mining District (Monte Amiata, Tuscany, Italy)." *Ore Geology Reviews* 41, no. 1: 35–48.

Bulian, F., A. Genesini, F. Marra, D. Scarponi, and P. Vannoli. 2024. "New Biostratigraphic and Paleoecologic Data on the Pliocene-Pleistocene Paleogeographic Evolution of the Northeastern Coastal Area of the Central Tyrrhenian Sea (Italy)." *Quaternary International* 692: 1–20.

Bulian, F., F. Marra, L. Monaco, et al. 2024. "$^{40}Ar/^{39}Ar$ Geochronologic and Paleoenvironmental Constraints to Glacial Termination III and MIS 7e, 7c, and 7a Sea Level Fluctuations on the Tyrrhenian Sea Coast of Italy." *Global and Planetary Change* 242: 104594.

Buttinelli, M., C. Chiarabba, M. Anselmi, I. Bianchi, D. De Rita, and F. Quattrocchi. 2014. "Crustal Structure of Northern Latium (Central Italy) From Receiver Functions Analysis: New Evidences of a Post-Collisional Back-Arc Margin Evolution." *Tectonophysics* 621: 148–158.

Buttinelli, M., F. Mazzarini, G. Musumeci, et al. 2024. "Tectonic-Sedimentary Evolution of the Tuscan Shelf (Italy): Seismic-Stratigraphic/Structural Analysis of Neogenic Succession in the Tyrrhenian Sea Between Elba Island and Monte Argentario Promontory." *Tectonophysics* 873: 230211.

Caneva, G., D. Isola, H. J. Lee, and Y. J. Chung. 2020. "Biological Risk for Hypogea: Shared Data From Etruscan Tombs in Italy and Ancient Tombs of the Baekje Dynasty in Republic of Korea." *Applied Sciences* 10, no. 17: 6104.

Carannante, G., M. Esteban, J. D. Milliman, and L. Simone. 1988. "Carbonate Lithofacies as Paleolatitude Indicators: Problems and Limitations." *Sedimentary Geology* 60, no. 1–4: 333–346.

Carboni, M. G., I. Palagi, L. Palieri, I. Raffi, and A. Sposato. 1994. "Dati Preliminari Sull'evoluzione Geologica Della Fascia Costiera del Lazio Settentrionale Durante il Pliocene." *Memorie Descrittive Della Carta Geologica D'italia* 49: 177–188.

Cardello, G. L., and C. Doglioni. 2015. "From Mesozoic Rifting to Apennine Orogeny: The Gran Sasso Range (Italy)." *Gondwana Research* 27, no. 4: 1307–1334.

Cardello, G. L., L. Tomassetti, I. Cornacchia, et al. 2022. "The Tethyan and Tyrrhenian Margin Record of the Central Apennines: A Guide With Insights From Stratigraphy, Tectonics, and Hydrogeology." *Geological Field Trips and Maps* 14, no. 2.2: 1–113.

Carminati, E., L. Corda, G. Mariotti, A. Scifoni, and F. Trippetta. 2013. "Mesozoic Syn-and Postrifting Evolution of the Central Apennines, Italy: The Role of Triassic Evaporites." *Journal of Geology* 121, no. 4: 327–354.

Carminati, E., and C. Doglioni. 2005. "Mediterranean Tectonics." In *Encyclopedia of Geology*, vol. 2, 135–146. Elsevier.

Catalano, R., E. Di Stefano, A. Sulli, F. P. Vitale, S. Infuso, and P. R. Vail. 1998. "Sequences and Systems Tracts Calibrated by High-Resolution Biochronostratigraphy: The Central Mediterranean Plio-Pleistocene Record." In *Mesozoic–Cenozoic Sequence Stratigraphy of European Basins*, edited by P. C. De Graciansky, J. Hardenbol, T. Jacquin, and P. R. Vail, vol. 60, 155–177. SEPM Special Publications.

Cataldi, M. 1993. "Tarquinia." *Quasar.* 23.

Chiarabba, C., I. Menichelli, I. Bianchi, G. Giacomuzzi, and P. De Gori. 2023. "Continental Subduction of Adria in the Apennines and Relation With Seismicity and Hazard." *Frontiers in Earth Science* 11: 1253443.

Chiarella, D., and S. G. Longhitano. 2012. "Distinguishing Depositional Environments in Shallow-Water Mixed, Bio-Siliciclastic Deposits on the Basis of the Degree of Heterolithic Segregation (Gelasian, Southern Italy)." *Journal of Sedimentary Research* 82, no. 12: 969–990.

Chiarella, D., S. G. Longhitano, L. Sabato, and M. Tropeano. 2012. "Sedimentology and Hydrodynamics of Mixed (Siliciclastic-Bioclastic) Shallow-Marine Deposits of Acerenza (Pliocene, Southern Apennines, Italy)." *Italian Journal of Geosciences* 131, no. 1: 136–151.

Chiarella, D., S. G. Longhitano, and M. Tropeano. 2017. "Types of Mixing and Heterogeneities in Siliciclastic-Carbonate Sediments." *Marine and Petroleum Geology* 88: 617–627.

Chiarella, D., S. G. Longhitano, and M. Tropeano. 2019. "Different Stacking Patterns Along an Active Fold-and-Thrust Belt—Acerenza Bay, Southern Apennines (Italy)." *Geology* 47, no. 2: 139–142.

Chiocchini, U., and F. Castaldi. 2009. "Caratteri Sedimentologici e Composizionali Delle Ghiaie del Sintema di Poggio Martino, Bacino Plio-Pleistocenico di Tarquinia, Italia Centrale." *Italian Journal of Geosciences. Bollettino Societa Geologica Italiana* 128: 695–713.

Chiocchini, U., and M. Potetti. 1998. "Caratteri Sedimentologici e Stratigrafici Delle Calcareniti di Tarquinia (Provincia di Viterbo)." *Bollettino del Servizio Geologico D'italia* 117: 33–52.

Chiocci, F. L., and L. Orlando. 1996. "Lowstand Terraces on Tyrrhenian Sea Steep Continental Slopes." *Marine Geology* 134, no. 1–2: 127–143.

Colalongo, M. L., G. Pasini, and L. Carobene. 1973. "Su Alcune Sezioni Neogeniche Presso la Costa Tirrenica tra Salerno e Livorno." *Giornale di Geologia* 39, no. 1: 101–113 Bologna.

Colella, A., and F. P. Vitale. 1998. "Eustacy, Tectonics and Their Controls on the Depositional Patterns of Clinostrati Wed Shoreface Carbonates (Late Pliocene, Sicily)." In *Strata and Sequences on Shelves and Slopes, SEPM, Research Conference, Catania-Sicily, September 1998, Excursion Guidebook*, edited by A. Colella, 29–69. Iris Unibas.

Coletti, G., G. Bosio, and A. Collareta. 2021. "Lower Pliocene Barnacle Facies of Western Liguria (NW Italy): A Peek Into a Warm Past and a Glimpse of Our Incoming Future." *Rivista Italiana di Paleontologia e Stratigrafia* 127, no. 1: 103–131.

Consorti, L., M. Sabbatino, and M. Parente. 2020. "Insights on the Paleoecology of Ammonia (Foraminifera, Rotalioidea) From Miocene Carbonates of Central and Southern Apennines (Italy)." *Palaeogeography, Palaeoclimatology, Palaeoecology* 562: 110105.

Conti, M. A., G. Parisi, and U. Nicosia. 1983. "Un Orizzonte ad *Amphistegina* nel Pliocene di Orvieto e sue Implicazioni Neotettoniche." *Bollettino Della Società Geologica Italiana* 102: 112–113 Roma.

Cosentino, A., and S. Giacobbe. 2006. "A Case Study of Mollusc and Polychaete Soft-Bottom Assemblages Submitted to Sedimentary Instability in the Mediterranean Sea." *Marine Ecology* 27, no. 2: 170–183.

13652117, 2026, 3, Downloaded from https://onlinelibrary.wiley.com/doi/10.1111/bre.70109 by University Di Roma La Sapienza, Wiley Online Library on [05/05/2026]. See the Terms and Conditions (https://onlinelibrary.wiley.com/terms-and-conditions) on Wiley Online Library for rules of use; OA articles are governed by the applicable Creative Commons License

Cosentino, D., P. Cipollari, P. Marsili, and D. Scrocca. 2010. "Geology of the Central Apennines: A Regional Review." *Journal of the Virtual Explorer* 36, no. 11: 1–37.

Di Bella, L., M. G. Carboni, and J. Pignatti. 2005. "Paleoclimatic Significance of the Pliocene *Amphistegina* Levels From the NE Tyrrhenian Margin of Central Italy." *Bollettino Della Societa Paleontologica Italiana* 44, no. 3: 219.

Di Stefano, A., N. Baldassini, I. Raffi, et al. 2023. "Neogene-Quaternary Mediterranean Calcareous Nannofossil Biozonation and Biochronology: A Review." *Stratigraphy* 20, no. 4: 259–302.

Doglioni, C. 1991. "A Proposal for the Kinematic Modelling of W-Dipping Subductions-Possible Applications to the Tyrrhenian-Apennines System." *Terra Nova* 3, no. 4: 423–434.

Dorsey, R. J. 1997. "Origin and Significance of Rhodolith-Rich Strata in the Punta El Bajo Section, Southeastern Pliocene Loreto Basin." In *Pliocene Carbonates and Related Facies Flanking the Gulf of California, Baja California, Mexico: Boulder, Colorado*, edited by M. E. Johnson and J. Ledesma-Vásquez, vol. 318, 119–126. Geological Society of America Special Paper.

Dupuy, C., L. Rossignol, E. Geslin, and P. Y. Pascal. 2010. "Predation of Mudflat Meio-Macrofaunal Metazoans by a Calcareous Foraminifer, *Ammonia tepida* (Cushman, 1926)." *Journal of Foraminiferal Research* 40, no. 4: 305–312.

Faccenna, C., P. Davy, J. P. Brun, et al. 1996. "The Dynamics of Back-Arc Extension: An Experimental Approach to the Opening of the Tyrrhenian Sea." *Geophysical Journal International* 126, no. 3: 781–795.

Fazzini, P., M. Gelmini, M. P. Mantovani, and M. Pellegrini. 1972. "Geologia dei Monti Della Tolfa (Lazio Settentrionale, Province di Viterbo e di Roma)." *Memorie della Societa Geologica Italiana* 21: 65–144.

Fornos, J. J., and W. M. Ahr. 1997. "Temperate Carbonates on a Modern, Low-Energy, Isolated Ramp; the Balearic Platform, Spain." *Journal of Sedimentary Research* 67, no. 2: 364–373.

Funiciello, R., E. Locardi, and M. Parotto. 1976. "Lineamenti Geologici Dell'area Sabatina Orientale." *Bollettino Della Società Geologica Italiana* 95: 831–849.

Gaglianone, G., M. Brandano, and G. Mateu-Vicens. 2017. "The Sedimentary Facies of *Posidonia oceanica* Seagrass Meadows From the Central Mediterranean Sea." *Facies* 63, no. 4: 28.

Garcia-Castellanos, D., A. Micallef, F. Estrada, et al. 2020. "The Zanclean Megaflood of the Mediterranean–Searching for Independent Evidence." *Earth-Science Reviews* 201: 103061.

Ghinassi, M. 2007. "Pliocene Alluvial to Marine Deposits of the Val D'orcia Basin (Northern Apennines, Italy): Sequence Stratigraphy and Basin Analysis." *Rivista Italiana di Paleontologia e Stratigrafia* 113: 459–472.

Gil-Gil, J., A. Bretones, C. Boix, and J. F. García-Hidalgo. 2024. "Evolution of Coniacian Facies and Environments in the Iberian Basin: A Longshore Current Controlling Siliciclastic Sand Distribution on a Carbonate Platform." *Facies* 70, no. 2: 7.

Grémare, A., R. Sardá, L. Medernach, et al. 1998. "On the Dramatic Increase of *Ditrupa arietina* O. F. Müller (Annelida: Polychaeta) Along Both the French and the Spanish Catalan Coasts." *Estuarine, Coastal and Shelf Science* 47, no. 4: 447–457.

Halfar, J., J. C. Ingle Jr, and L. Godinez-Orta. 2004. "Modern Non-Tropical Mixed Carbonate-Siliciclastic Sediments and Environments of the Southwestern Gulf of California, Mexico." *Sedimentary Geology* 165, no. 1-2: 93–115.

Halfar, J., and M. Mutti. 2005. "Global Dominance of Coralline Red-Algal Facies: A Response to Miocene Oceanographic Events." *Geology* 33, no. 6: 481–484.

Hansen, K. S. 1999. "Development of a Prograding Carbonate Wedge During Sea Level Fall: Lower Pleistocene of Rhodes, Greece." *Sedimentology* 46, no. 3: 559–576.

Haynes, J. R. 1992. "Supposed Pronounced Ecophenotypy in Foraminifera." *Journal of Micropalaeontology* 11, no. 1: 59–63.

Healy, D., R. E. Rizzo, D. G. Cornwell, et al. 2017. "FracPaQ: A MATLAB Toolbox for the Quantification of Fracture Patterns." *Journal of Structural Geology* 95: 1–16.

Héquette, A., M. Desrosiers, P. R. Hill, and D. L. Forbes. 2001. "The Influence of Coastal Morphology on Shoreface Sediment Transport Under Storm-Combined Flows, Canadian Beaufort Sea." *Journal of Coastal Research* 17: 507–516.

Hottinger, L. 1983. "Neritic Macroid Genesis, an Ecological Approach." In *Coated Grains*, 38–55. Springer Berlin Heidelberg.

Iaccarino, S. 1985. "Mediterranean Miocene and Pliocene Planktic Foraminifera." In *Plankton Stratigraphy*, edited by H. M. Bolli, J. B. Saunders, and K. Perch-Nielsen, 283–314. Cambridge.

Iaccarino, S., I. Premoli Silva, M. Biolzi, et al. 2007. *Practical Manual of Neogene Planktonic Foraminifera*, 1–180. Università di Perugia Press.

Johnson, M. E. 2026. "Rhodoliths as Global Contributors to a Carbonate Ecosystem Dominated by Coralline Red Algae With an Established Fossil Record." *Journal of Marine Science and Engineering* 14, no. 2: 169.

Johnson, M. E., D. M. Perez, and B. G. Baarli. 2012. "Rhodolith Stranding Event on a Pliocene Rocky Shore From Isla Cerralvo in the Lower Gulf of California (Mexico)." *Journal of Coastal Research* 28, no. 1: 225–233.

Jolivet, L., C. Faccenna, B. Goffé, et al. 1998. "Midcrustal Shear Zones in Postorogenic Extension: Example From the Northern Tyrrhenian Sea." *Journal of Geophysical Research: Solid Earth* 103, no. B6: 12123–12160.

Jorissen, F. J. 1988. "Benthic Foraminifera From the Adriatic Sea: Principles of Phenotypic Variation." PhD diss., Utrecht University.

Labrune, C., J. M. Amouroux, R. Sarda, et al. 2006. "Characterization of the Ecological Quality of the Coastal Gulf of Lions (NW Mediterranean). A Comparative Approach Based on Three Biotic Indices." *Marine Pollution Bulletin* 52, no. 1: 34–47.

Likorish, W. H., and R. W. H. Butler. 1996. "Fold Amplication and Parasequence Stacking Patterns in Syntectonic Shoreface Carbonates." *Geological Society of America Bulletin* 108: 966–977.

Lirer, F., L. M. Foresi, S. M. Iaccarino, et al. 2019. "Mediterranean Neogene Planktonic Foraminifer Biozonation and Biochronology." *Earth-Science Reviews* 196: 13. https://doi.org/10.1016/j.earscirev.2019.05.013.

Locardi, E. 1986. "Tyrrhenian Volcanic Arcs: Volcano-Tectonics, Petrogenesis and Economic Aspects." *Developments in Geotectonics* 21: 351–373 Elsevier.

Malinverno, A., and W. B. Ryan. 1986. "Extension in the Tyrrhenian Sea and Shortening in the Apennines as Result of Arc Migration Driven by Sinking of the Lithosphere." *Tectonics* 5, no. 2: 227–245.

Manatschal, G., P. Chenin, J. F. Ghienne, C. Ribes, and E. Masini. 2022. "The Syn-Rift Tectono-Stratigraphic Record of Rifted Margins (Part I): Insights From the Alpine Tethys." *Basin Research* 34, no. 1: 457–488.

Mariani, M., and R. Prato. 1988. "I Bacini Neogenici Costieri del Margine Tirrenico: Approccio Sismico-Stratigrafico." *Memorie della Societa Geologica Italiana* 41: 519–531.

Marrack, E. C. 1999. "The Relationship Between Water Motion and Living Rhodolith Beds in the Southwestern Gulf of California, Mexico." *PALAIOS* 14: 159–171.

MartÍn, J. M., J. C. Braga, J. Aguirre, and C. Betzler. 2004. "Contrasting Models of Temperate Carbonate Sedimentation in a Small Mediterranean Embayment: The Pliocene Carboneras Basin, SE Spain." *Journal of the Geological Society* 161, no. 3: 387–399.

13652117, 2026, 3, Downloaded from https://onlinelibrary.wiley.com/doi/10.1111/bre.70109 by University Di Roma La Sapienza, Wiley Online Library on [05/05/2026]. See the Terms and Conditions (https://onlinelibrary.wiley.com/terms-and-conditions) on Wiley Online Library for rules of use; OA articles are governed by the applicable Creative Commons License

Massari, F., and F. Chiocci. 2006. "Biocalcarenite and Mixed Cool-Water Prograding Bodies of the Mediterranean Pliocene and Pleistocene: Architecture, Depositional Setting and Forcing Factors." In *Cool-Water Carbonates: Depositional Systems and Palaeoenvironmental Controls*, edited by H. M. Pedley and G. Carannante, vol. 255, 95–120. Geological Society of London, Special Publication.

Massari, F., and A. D'Alessandro. 2010. "Icehouse, Cool-Water Carbonate Ramps: The Case of the Upper Pliocene Capodarso Fm (Sicily): Role of Trace Fossils in the Reconstruction of Growth Stages of Prograding Wedges." *Facies* 56, no. 1: 47–58.

Massari, F., and A. D'Alessandro. 2012. "Facies Partitioning and Sequence Stratigraphy of a Mixed Siliciclastic-Carbonate Ramp Stack in the Gelasian of Sicily (S Italy): A Potential Model for Icehouse, Distally-Steepened Heterozoan Ramps." *Rivista Italiana di Paleontologia e Stratigrafia* 118, no. 3: 503–534.

Massari, F., D. Rio, M. Sgavetti, et al. 2002. "Interplay Between Tectonics and Glacio-Eustasy: Pleistocene Succession of the Crotone Basin, *Calabria*." *Geological Society of America Bulletin* 114: 1183–1209.

Mateu-Vicens, G., M. Brandano, G. Gaglianone, and A. Baldassarre. 2012. "Seagrass-Meadow Sedimentary Facies in a Mixed Siliciclastic–Carbonate Temperate System in the Tyrrhenian Sea (Pontinian Islands, Western Mediterranean)." *Journal of Sedimentary Research* 82, no. 7: 451–463.

Mazzini, I., P. Paccara, C. Petronio, and R. Sardella. 2000. "Geological Evolution and Biochronological Evidences of the Monte Riccio Section (Tarquinia, Central Italy)." *Rivista Italiana di Paleontologia e Stratigrafia* 106, no. 2: 247–256.

Miller, K. G., J. V. Browning, W. J. Schmelz, R. E. Kopp, G. S. Mountain, and J. D. Wright. 2020. "Cenozoic Sea-Level and Cryospheric Evolution From Deep-Sea Geochemical and Continental Margin Records." *Science Advances* 6, no. 20: eaaz1346.

Morton, B., and A. Salvador. 2009. "The Biology of the Zoning Subtidal Polychaete *Ditrupa arietina* (Serpulidae) in the Açores, Portugal, With a Description of the Life History of Its Tube." *Acoreana Suplemento* 6: 145–156.

Mount, J. F. 1984. "Mixing of Siliciclastic and Carbonate Sediments in Shallow Shelf Environments." *Geology* 12: 432–435.

Murray, J. W. 2006. *Ecology and Applications of Benthic Foraminifera*. Cambridge University Press.

Nalin, R., M. Ghinassi, and D. Basso. 2010. "Onset of Temperate Carbonate Sedimentation During Transgression in a Low-Energy Siliciclastic Embayment (Pliocene of the Val d'Orcia Basin, Tuscany, Italy)." *Facies* 56: 353–368.

Nalin, R., M. Ghinassi, L. M. Foresi, and E. Dallanave. 2016. "Carbonate Deposition in Restricted Basins: A Pliocene Case Study From the Central Mediterranean (Northwestern Apennines), Italy." *Journal of Sedimentary Research* 86, no. 3: 236–267.

Ortner, H., F. Reiter, and P. Acs. 2002. "Easy Handling of Tectonic Data: The Programs TectonicVB for Mac and TectonicsFP for Windows." *Computers and Geosciences* 28, no. 10: 1193–1200.

Pascucci, V. 2005. "Neogene Evolution of the Viareggio Basin, Northern Tuscany (Italy)." *GeoActa* 4: 123–138.

Pascucci, V., A. Costantini, I. P. Martini, and R. Dringoli. 2006. "Tectono-Sedimentary Analysis of a Complex, Extensional, Neogene Basin Formed on Thrust-Faulted, Northern Apennines Hinterland: Radicofani Basin, Italy." *Sedimentary Geology* 183, no. 1–2: 71–97.

Pascucci, V., and I. P. Martini. 2002. "Seismic Stratigraphy of the Miocene–Pleistocene Sedimentary Basins of the Northern Tyrrhenian Sea and Western Tuscany (Italy)." *Basin Research* 11, no. 4: 337–356.

Patacca, E., and P. Scandone. 1989. "Post-Tortonian Mountain Building in the Apennines. The Role of the Passive Sinking of a Relic Lithospheric Slab." *Atti Dei Convegni Lincei* 80: 157–176.

Pomar, L. 2001. "Types of Carbonate Platforms: A Genetic Approach." *Basin Research* 13, no. 3: 313–334.

Pomar, L. 2020. "Carbonate Systems." In *Regional Geology and Tectonics*, 235–311. Elsevier.

Pomar, L., J. I. Baceta, P. Hallock, G. Mateu-Vicens, and D. Basso. 2017. "Reef Building and Carbonate Production Modes in the West-Central Tethys During the Cenozoic." *Marine and Petroleum Geology* 83: 261–304.

Pomar, L., and C. G. S. C. Kendall. 2008. "Architecture of Carbonate Platforms: A Response to Hydrodynamics and Evolving Ecology." In *Controls on Carbonate Platform and Reef Development*, edited by J. Lukasik and A. Simo, vol. 89, 187–216. SEPM Special Publication.

Pomar, L., A. Obrador, and H. Westphal. 2002. "Sub-Wavebase Cross-Bedded Grainstones on a Distally Steepened Carbonate Ramp, Upper Miocene, Menorca." *Spain. Sedimentology* 49, no. 1: 139–169.

Pomar, L., and M. Tropeano. 2001. "The Calcarenite di Gravina Formation in Matera (Southern Italy): New Insights for Coarse-Grained, Largescale, Cross-Bedded Bodies Encased in Offshore Deposits." *American Association of Petroleum Geologists* 85: 661–689.

Puga-Bernabéu, Á., J. M. Martín, and J. C. Braga. 2007. "Tsunami-Related Deposits in Temperate Carbonate Ramps, Sorbas Basin, Southern Spain." *Sedimentary Geology* 199, no. 3–4: 107–127.

Quiquerez, A., and G. Dromart. 2006. "Environmental Control on Granular Clinoforms of Ancient Carbonate Shelves." *Geological Magazine* 143, no. 3: 343–365.

Read, J. F. 1998. "Phanerozoic Carbonate Ramps From Greenhouse, Transitional, and Ice-House Worlds: Clues From Weld and Modelling Studies." In *Carbonate Ramps*, edited by V. P. Wright and T. P. Burchette, vol. 149, 107–136. Geological Society, London, Special Publications.

Rebelo, A. C., M. W. Rasser, A. Kroh, et al. 2016. "Rocking Around a Volcanic Island Shelf: Pliocene Rhodolith Beds From Malbusca, Santa Maria Island (Azores, NE Atlantic)." *Facies* 62, no. 3: 22.

Rebelo, A. C., A. Uchman, M. E. Johnson, et al. 2025. "Rhodoliths and Trace Fossils Record Stabilization of a Fan-Delta System: An Example From the Mio-Pliocene Deposits of Gran Canaria (Canary Islands, Spain)." *Journal of Palaeogeography* 14: 100266.

Reijmer, J. J. 2021. "Marine Carbonate Factories: Review and Update." *Sedimentology* 68, no. 5: 1729–1796.

Rouchy, J. M., F. Orszag-Sperber, M. M. Blanc-Valleron, et al. 2001. "Paleoenvironmental Changes at the Messinian–Pliocene Boundary in the Eastern Mediterranean (Southern Cyprus Basins): Significance of the Messinian Lago-Mare." *Sedimentary Geology* 145, no. 1–2: 93–117.

Roveri, M., and M. Taviani. 2003. "Calcarenite and Sapropel Deposition in the Mediterranean Pliocene: Shallow- and Deep-Water Record of Astronomically Driven Climatic Events." *Terra Nova* 15: 279–286.

Sartori, R., L. Torelli, N. Zitellini, G. Carrara, M. Magaldi, and P. Mussoni. 2004. "Crustal Features Along a W–E Tyrrhenian Transect From Sardinia to Campania Margins (Central Mediterranean)." *Tectonophysics* 383, no. 3–4: 171–192.

Savelli, C. 2002. "Time–Space Distribution of Magmatic Activity in the Western Mediterranean and Peripheral Orogens During the Past 30 ma (a Stimulus to Geodynamic Considerations)." *Journal of Geodynamics* 34, no. 1: 99–126.

Schlager, W. 2003. "Benthic Carbonate Factories of the Phanerozoic." *International Journal of Earth Sciences* 92, no. 4: 445–464.

Schlager, W. 2005. *Carbonate Sedimentology and Sequence Stratigraphy (No. 8)*. SEPM Society for Sedimentary Geology.

Schneider von Deimling, J., J. Hoffmann, J. Geersen, et al. 2023. "Millions of Seafloor Pits, Not Pockmarks, Induced by Vertebrates in the North Sea." *Communications Earth & Environment* 4, no. 1: 478.

13652117, 2026, 3, Downloaded from https://onlinelibrary.wiley.com/doi/10.1111/bre.70109 by University Di Roma La Sapienza, Wiley Online Library on [05/05/2026]. See the Terms and Conditions (https://onlinelibrary.wiley.com/terms-and-conditions) on Wiley Online Library for rules of use; OA articles are governed by the applicable Creative Commons License

Schwarz, E., G. D. Veiga, G. Álvarez Trentini, M. F. Isla, and L. A. Spalletti. 2018. "Expanding the Spectrum of Shallow-Marine, Mixed Carbonate–Siliciclastic Systems: Processes, Facies Distribution and Depositional Controls of a Siliciclastic-Dominated Example." *Sedimentology* 65, no. 5: 1558–1589.

Steneck, R. S. 1986. "The Ecology of Coralline Algal Crusts: Convergent Patterns and Adaptative Strategies." *Annual Review of Ecology and Systematics* 17: 273–303.

Swift, D. J. P., and J. A. Thorne. 1991. "Sedimentation on Continental Margins, I: A General Model for Shelf Sedimentation." In *Shelf Sand and Sandstone Bodies*, edited by D. J. P. Swift, G. F. Oertel, R. W. Tillman, and J. A. Thorne, vol. 14, 3–31. International Association of Sedimentologists (IAS) Special Publications.

Tavani, S., G. L. Cardello, G. Vignaroli, et al. 2021. "Segmentation of the Apenninic Margin of the Tyrrhenian Back-Arc Basin Forced by the Subduction of an Inherited Transform System." *Tectonics* 40, no. 9: e2021TC006770.

Tavani, S., K. Ogata, F. Vinci, et al. 2023. "Post-Rift Aptian-Cenomanian Extension in Adria, Insight From the km-Scale Positano-Vico Equense Syn-Sedimentary Fault." *Journal of Structural Geology* 168: 104820.

Taylor, A. M., and R. Goldring. 1993. "Description and Analysis of Bioturbation and Ichnofabric." *Journal of the Geological Society* 150, no. 1: 141–148.

Tomassetti, L., and M. Brandano. 2013. "Sea Level Changes Recorded in Mixed Siliciclastic–Carbonate Shallow-Water Deposits: The Cala di Labra Formation (Burdigalian, Corsica)." *Sedimentary Geology* 294: 58–67.

Torfstein, A., and J. Steinberg. 2020. "The Oligo–Miocene Closure of the Tethys Ocean and Evolution of the Proto-Mediterranean Sea." *Scientific Reports* 10, no. 1: 13817.

Tortora, P. 1996. "Depositional and Erosional Coastal Processes During the Last Postglacial Sea-Level Rise; an Example From the Central Tyrrhenian Continental Shelf (Italy)." *Journal of Sedimentary Research* 66, no. 2: 391–405.

Vitale, F. P. 1998. "Stacking Pattern and Tectonics: Weld Evidence From Pliocene Growth Folds of Sicily (Central Mediterranean) Plio-Pleistocene Record." In *Mesozoic–Cenozoic Sequence Stratigraphy of European Basins*, edited by P. C. De Graciansky, J. Hardenbol, T. Jacquin, and P. R. Vail, vol. 60, 181–199. SEPM Special Publications.

Walker, L. J., B. H. Wilkinson, and L. C. Ivany. 2002. "Continental Drift and Phanerozoic Carbonate Accumulation in Shallow-Shelf and Deep-Marine Settings." *Journal of Geology* 110: 75–87.

Wright, L. D., J. D. Boon, S. C. Kim, and J. H. List. 1991. "Modes of Cross-Shore Sediment Transport on the Shoreface of the Middle Atlantic Bight." *Marine Geology* 96: 19–51.

Zecchin, M. 2017. "High-Resolution Sequence Stratigraphy of Clastic Shelves VI: Mixed Siliciclastic-Carbonate Systems." *Marine and Petroleum Geology* 88: 712–723.

13652117, 2026, 3, Downloaded from https://onlinelibrary.wiley.com/doi/10.1111/bre.70109 by University Di Roma La Sapienza, Wiley Online Library on [05/05/2026]. See the Terms and Conditions (https://onlinelibrary.wiley.com/terms-and-conditions) on Wiley Online Library for rules of use; OA articles are governed by the applicable Creative Commons License